Field trip A2 – Red Istria : Western Istrian Anticline as an ideal natural laboratory for the study of the regional unconformities in carbonate rocks

Durn, Goran; Perković, Ivor; Mileusnić, Marta; Vlahović, Igor; Ružičić, Stanko; Matešić, Darko; Cvetko Tešović, Blanka; Martinuš, Maja; Rubinić, Vedran; Razum, Ivan; ...

FIELD TRIP A2

RED ISTRIA

FIELD TRIP A2 – RED ISTRIA

WESTERN ISTRIAN ANTICLINE AS AN IDEAL NATURAL LABORATORY FOR THE STUDY OF THE REGIONAL UNCONFORMITIES IN CARBONATE ROCKS

Goran Durn[1], Ivor Perković[1], Marta Mileusnić[1], Igor Vlahović[1], Stanko Ružičić[1], Darko Matešić[1], Blanka Cvetko Tešović[2], Maja Martinuš[2], Vedran Rubinić[3], Ivan Razum[4], Branimir Šegvić[5], Milan Mihovilović[6], Sergej Zvocak[7]

[1] University of Zagreb, Faculty of Mining, Geology and Petroleum Engineering, Pierottijeva 6, 10 000 Zagreb, Croatia
goran.durn@rgn.unizg.hr; ivor.perkovic@rgn.unizg.hr; marta.mileusnic@rgn.unizg.hr; igor.vlahovic@rgn.unizg.hr; stanko.ruzicic@rgn.unizg.hr; darko.matesic@rgn.unizg.hr

[2] University of Zagreb, Faculty of Science, Department of Geology, Horvatovac 102b, 10 000 Zagreb, Croatia
bcvetko@geol.pmf.unizg.hr; maja.martinus@geol.pmf.unizg.hr

[3] University of Zagreb, Faculty of Agriculture, Svetošimunska cesta 102a, 10 000 Zagreb, Croatia
vrubinic@agr.hr

[4] Croatian Natural History Museum, Demetrova 1, 10 000, Zagreb, Croatia
ivan.razum@hpm.hr

[5] Texas Tech University, Department of Geosciences, Mail Stop 1053, Lubbock, TX 79409-1053, USA
branimir.segvic@ttu.edu

[6] GEO-5 d.o.o., Carera 59, 52 210 Rovinj, Croatia
rovinj.geo5@gmail.com

[7] Kamen d.d. za proizvodnju i obradu kamena, Trg slobode 2, 52 000 Pazin, Croatia
sergej.zvocak@kamen.hr

INTRODUCTION

Erosional unconformities typically represent long periods of subaerial erosion associated with loss of rock records, vadose diagenetic and/or pedogenetic alteration, and the formation of surface and subsurface karst (ALONSO-ZARZA & WRIGHT, 2010). Depending on their origin (e.g., tectonically controlled uplift and/or associated relative sea-level fall), climate, and duration of subaerial exposure, unconformities in shallow-water carbonate successions can be associated with different phenomena and/or materials. Due to the formation of surface and subsurface karst, unconformities may be characterised by various karst features (e.g., cavities, dolines, sinkholes, caves, canyons). In addition to various deposits (e.g., laminar rootcrete, breccias, carbonate lithoclasts), unconformities in shallow-water carbonate successions can be accompanied by various palaeosols, soils, soil-derived sediments, and/or pedo-sedimentary complexes. According to MINDSZENTY (2004), these materials may be associated with long-lasting (tectonically controlled) subaerial exposures at major regional unconformities and/or to cyclically organised sequences where marine sedimentation is repeatedly interrupted by shorter or longer episodes of nondeposition and subaerial exposure (controlled by intrinsic or extrinsic factors).

The Adriatic Carbonate Platform (AdCP – see VLAHOVIĆ et al., 2005 and references therein) is one of the best preserved Peri-Mediterranean platforms, located on a stable part of the Adria Microplate characterised by almost continuous carbonate deposition since the Middle Permian. This long-lasting shallow marine carbonate deposition is the result of a combination of (i) stable subsidence, (ii) relative isolation from continental influences, and (iii) palaeogeographic position between the equator and 30° N latitude until the end of the Cretaceous, i.e., within a climatic belt ideal for massive carbonate production. Unlike other parts of the AdCP, the area of the Western Istrian Anticline, the adjacent Pazin Flysch Basin and the Savudrija–Buzet Anticline (which together make up most of Istria, with the exception of the Ćićarija Mt. in its northernmost part and the Učka Mt. along its northeastern and eastern margins) does not belong to the Dinaric mountain belt, but is part of the undeformed foreland of the Adria Microplate (SCHMID et al., 2008; HANDY et al., 2010), i.e. its tectonically much less disturbed part. During the Jurassic and Cretaceous periods, Istria formed the northwestern part of the AdCP and was subsequently covered by Eocene deposits, especially in the northern and northeastern parts, followed by a thin layer of Quaternary deposits throughout the region.

Due to the particular palaeogeographic position of present-day Istria on the northwestern margin of the Adriatic Carbonate Platform, which was characterised by decreased subsidence rate, the Jurassic, Cretaceous, and Palaeogene Istrian successions generally have lower deposition rates, thinner deposits, and more pronounced unconformities compared to contemporaneous deposits in other parts of the AdCP. The particular geotectonic position of the Western Istrian Anticline, which includes most of Istria as an undeformed part of the Adria Microplate, resulted in relatively gentle tectonic deformation and thus very good preservation of original conditions, which allowed almost complete record of unconformities along the limbs of the anticline.

Succession of Istrian deposits can be divided into four megasequences, mostly composed of carbonate deposits (mostly limestones, interbedded with dolomites in some layers; VELIĆ et al., 1995, 2003): 1st Megasequence (lower Bathonian–lower Kimmeridgian); 2nd Megasequence (upper Tithonian–lower/upper Aptian); 3rd Megasequence (lower/upper Albian–upper Santonian); and 4th Megasequence (Eocene) (Fig. 1). The aforementioned megasequences were bound by regional unconformities characterised by significant stratigraphic hiatuses, leading to the formation of terrestrial deposits under different conditions. It is important to emphasise the influence of synsedimentary tectonics, which in the studied area started already in the Early Cretaceous (MATIČEC et al., 1996), resulting in the uplift of the Western Istrian Anticline core and the erosion and/or non-deposition of younger deposits, which significantly reduced the total cover of the underlying deposits.

Well-defined stratigraphic hiatuses of long duration and very gentle post-depositional tectonics allowed the formation of an ideal natural laboratory for the study of major long-lasting unconformities in carbonate rocks. Regional unconformities are characterised by different terrestrial materials (bauxites, palaeosols, terra rossa, pedo-sedimentary complexes, loess-palaeosol sequences) formed in specific palaeoenvironments.

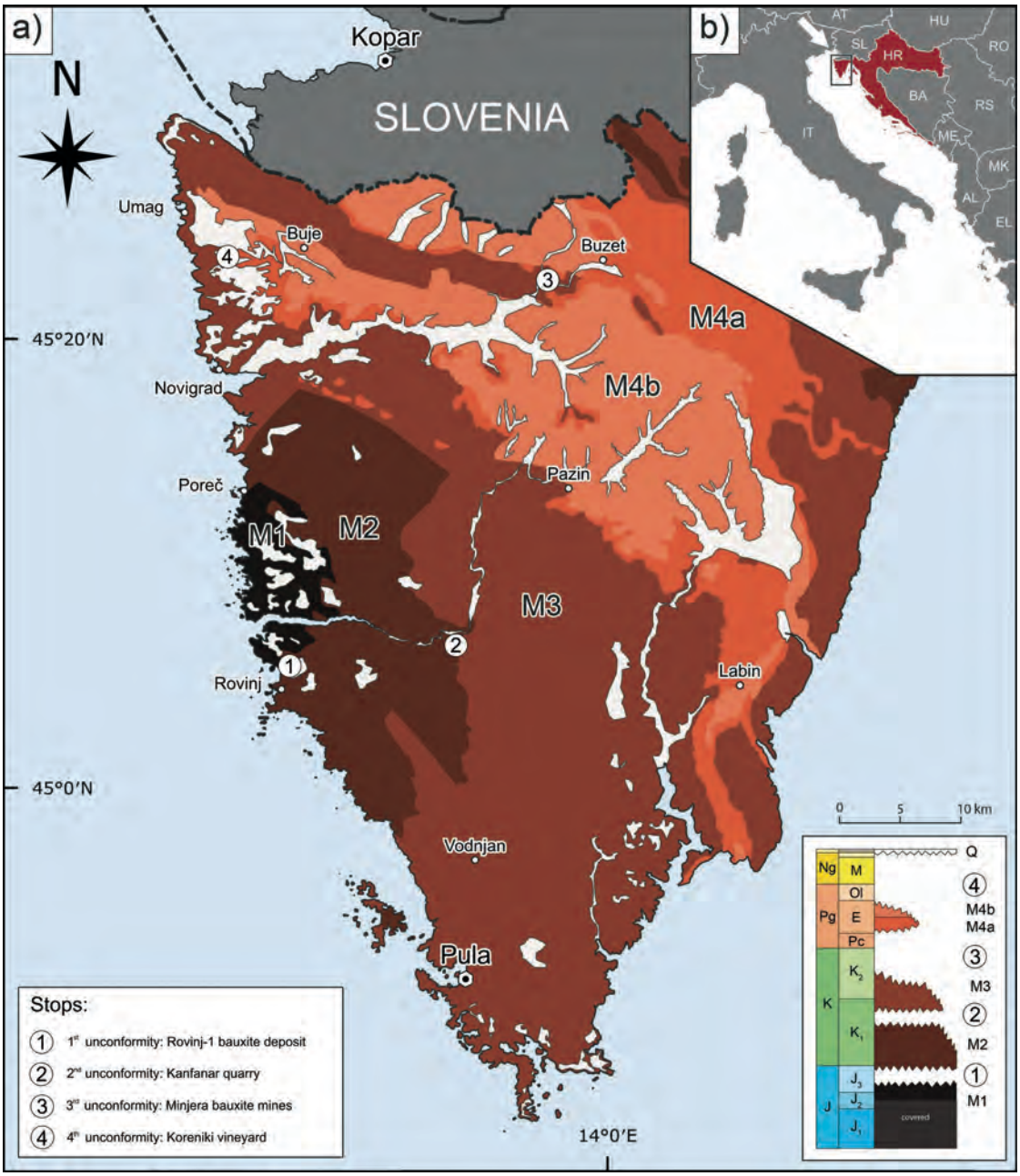

Fig. 1. (a) Map of the Istrian peninsula showing large-scale megasequences separated by regional unconformities, modified after Velić et al. (1995). Legend: M1 – 1st Megasequence (lower Bathonian–lower Kimmeridgian); M2 – 2nd Megasequence (upper Tithonian–lower/upper Aptian); M3 – 3rd Megasequence (lower/upper Albian–upper Santonian); M4a – Carbonate deposits of the 4th Megasequence (lower– middle Eocene); M4b – Clastic deposits of the 4th Megasequence (middle–upper Eocene); Q – Quaternary deposits. The excursion stops are marked with numbers 1 to 4. (b) Location map of Istria.

(A) Lowermost Kimmeridgian–upper Tithonian unconformity was of a relatively long duration (at least 6 Ma – VELIĆ et al., 2003) and resulted in a strongly differentiated relief. This unconformity is accompanied by bauxites. Bauxites are humid-tropical weathering products, similar to ferrallitic soils, which require long-lasting (> 1 Ma) subaerial exposure to form. The occurrence of bauxites is therefore generally considered to indicate a long-lasting exposure and a hot, humid climate. RETALLACK (2010) pointed out that the abundance distribution of bauxites over geologic time shows a pronounced positive correlation with "greenhouse periods" in Earth history. According to D'ARGENIO & MINDSZENTY (1995), subaerial exposure favouring bauxitization on carbonate successions (karst bauxites) is almost always the result of tectonically controlled uplift and associated relative sea-level fall (which may or may not coincide with a lower-order eustatic event). Using studies of Cretaceous karst bauxites, MINDSZENTY (2016) showed that bauxite peaks coincide with globally high temperatures, concurrent eustatic sea-level highs, positive anomalies of global magmatic activity, and abundant oceanic anoxia. Although the likely palaeogeographic position of Istria during the Late Jurassic was within the intertropical belt (after CHANNELL, 1996; STAMPFLI & MOSAR, 1999), the mechanism that led to the sufficient duration of exposure deserves attention because it apparently counteracted the uniform thermal subsidence that is considered characteristic of most Jurassic peri-Adriatic carbonate platforms (e.g., BERNOULLI, 2001). It is likely that the main cause of such an event was large-scale compressional deformation caused by the obduction of ophiolites along the northeastern AdCP margin (SCHMID et al., 2008). The uppermost part of the bauxite is highly altered: its colour is greenish-grey to yellowish-white with vertical to subvertical extensions penetrating the underlying deep red bauxite (DURN et al., 2003). The nature of Fe mineral alteration is clearly redox-based and is closely related to the environmental changes that accompanied overburden deposition.

(B) Upper Aptian–upper Albian unconformity in Istria was of variable duration (11–19 Ma; VLAHOVIĆ et al., 2005) and is accompanied by greenish-grey clay occurring mainly in palaeokarst pits and coarse brecciated regolith (DURN et al., 2003). The thickness of the clays associated with this unconformity ranges from a few centimetres to 1 metre. Transition zones between the shallow-water carbonates and emerged parts of the platform are characterised by clay and marl deposition or by the formation of extensive coastal marshes with reductive conditions and deposition of black sediments (black pebbles). A weakly developed soil structure, the presence of root remains, burrows and channels, now filled mainly with pyrite framboids, nests containing faecal products of soil-dwelling fauna, and nodular pedofeatures indicate that they have been pedogenetically altered. Therefore, the colour of the palaeosols, the presence of root remains only in the upper part of the profile, and the large amount of pyrite framboids may indicate that they were probably seasonally marshy soils or permanently waterlogged soils (DURN et al., 2003).

(C) Upper Cenomanian/upper Santonian–lower Eocene unconformity was of a very long duration (from about 25 Ma in southern Istria and the Učka Mt. to 40 Ma in northern Istria). However, in western Istria, erosional remains of middle Eocene foraminiferal limestones were found at several sites overlying Lower Cretaceous limestones, indicating a possible stratigraphic hiatus of up to about 87 Ma (MATIČEC et al., 1996). During such a long hiatus, part of the succession could have been chemically and physically weathered, so the above duration of the hiatus is probably somewhat overestimated. Although this stratigraphic hiatus was extremely long, relatively thin deposits, mostly bauxite, formed in the lowermost parts of the palaeorelief. Their occurrence coincides with one of the most widespread bauxite events in the Peri-Mediterranean area. Bauxites of Palaeogene age are abundant from Hungary through Slovenia, Croatia, and Bosnia and Herzegovina to Albania and Greece, all belonging to the Apulian Promontory (Adriatic Microplate) palaeogeographic domain (BÁRDOSSY & DERCOURT, 1990). As with the Jurassic bauxites, the cover sequence also normally begins with a palustrine/lacustrine transitional facies. In association with the initial transgression, the introduction of stagnant pore water into the soil-derived sediment occurs at a stage when diffuse porosity throughout the deposit is not yet restricted and the iron oxide phases are still partially mineralized, so that the bauxite may well react with reducing fluids, resulting in large-scale alteration. This is the case with most of the bauxite deposits in the Minjera area. The famous pyritic bauxites, where whole bauxite bodies are thoroughly grey due to finely disseminated eogenetic pyrite, clearly show that in some deposits the above conditions were met when marine pore water came into contact with the unconsolidated bauxite (ŠINKOVEC et al., 1994).

(D) Upper Eocene–Recent unconformity was of a very long duration, even in the areas with the longest deposition – up to the flysch in the latest Eocene (resulting in a stratigraphic hiatus of about 35 Ma). However, on the limbs of the Western Istrian Anticline, the hiatus was longer due to synsedimentary tectonics, as there were probably no younger deposits than the Middle Eocene foraminifera limestones (40–45 Ma), while in the apical part there may have been no carbonate deposition since the Early Cretaceous time, so the duration of the stratigraphic hiatus could be more than 100 Ma. This unconformity is accompanied by different deposits and soils/palaeosols among which terra rossa, loess-palaeosol sequences and pedo-sedimentary complexes are predominant.

Field trip participants will visit four sites with different terrestrial materials associated with the four regional unconformities in the shallow-marine carbonate successions within the Western Istrian Anticline and the Savudrija–Buzet Anticline, serving as indicators of palaeoenvironment, palaeoclimate, and provenance: (1) Rovinj-1 bauxite open pit (the lowermost Kimmeridgian–upper Tithonian regional unconformity) with red, grey and white bauxite; (2) Kanfanar quarry (the upper Aptian–upper Albian regional unconformity) with greenish-grey clay as palaeosol;

(3) Minjera historic bauxite mine (the upper Cenomanian/upper Santonian–lower Eocene regional unconformity) with pyritic bauxite; (4) Koreniki vineyard (the upper Eocene–Recent regional unconformity) with terra rossa soil profile classified as Rhodic Lixisol according to the WRB system. Special attention will be given to the sedimentology, mineralogy, geochemistry and micromorphology of these materials. This excursion was prepared on the basis of investigations carried out within the WIANLab project. Some of the results that we will present during this excursion have been published this year. This refers mainly to site 4, where the results published in the article by DURN et al. (2023) will be presented.

STOP 1 – ROVINJ-1 BAUXITE DEPOSIT: LOWERMOST KIMMERIDGIAN–UPPER TITHONIAN UNCONFORMITY

The 1st stop represents one of the best outcrops of the 1st unconformity. The unconformity between the Oxfordian to lower Kimmeridgian and upper Tithonian carbonate deposits is marked with the formation of a large bauxite body up to 20 metres thick – the Rovinj-1 bauxite deposit (Fig. 2), which is currently the only operating bauxite mine in Croatia. However, the bauxite ore is not used for aluminium production due to its high silica content but is currently used as a secondary ore in the production of mineral wool. With estimated reserves of around 15 million tonnes, it is also one of the largest bauxite deposits in Croatia.

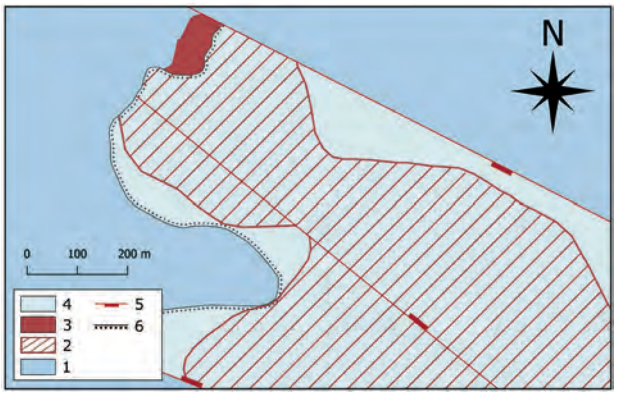

Fig. 2. Geological map of the Rovinj-1 deposit, based on the data provided by the GEO-5 company. Legend: 1 – Muča unit, 2 – extent of the bauxite body below the Kirmenjak unit, 3 –bauxite, 4 – Kirmenjak unit, 5 – normal faults, 6 – unconformity.

Regional and geotectonic setting

Rovinj bauxite represents one example of bauxite formation in the northern part of the Adriatic Carbonate Platform, since many other bauxite occurrences of the same age are documented in this area (TROJANOVIĆ, 1973; ŠINKOVEC, 1974; VELIĆ & TIŠLJAR, 1988). It is also a part of a much more widespread bauxite belt which formed during the Late Jurassic in the Tethyan realm. Karst bauxites of Upper Jurassic age can be found in Spain (MOLINA et al., 1991), Austria (STEINER et al., 2021), Slovenia (DOZET et al., 1993) and all the way to Montenegro (RADUSINOVIĆ et al., 2017; RADUSINOVIĆ & PAPADOPOULOS, 2021) and Greece (LASKOU & ECONOMOU-ELIOPOULOS, 2007; GAMALETSOS et al., 2017). The timing of this regional bauxitisation event coincides with higher temperatures recorded in the Late Jurassic (FRAKES et al., 1992; BRIGAUD et al., 2008; HAQ, 2018), as most of the Jurassic was characterised by coldhouse conditions (FRAKES et al., 1992). Since the sea level during the Late Jurassic was the highest during all of Jurassic (HAQ & AL-QAHTANI, 2005; HAQ, 2018), it is likely that the prolonged subaerial exposure required for bauxite formation was not a consequence of eustatic sea-level changes, but was of a tectonic nature. On the Adriatic Carbonate Platform this uplift was triggered in response to the overburden pressure generated by the oceanic crust during the obduction of the Vardar Ocean ophiolites in the Late Jurassic (SCHMID et al., 2008, 2020; VAN HINSBERGEN et al., 2020), which generated a flexural forebulge in the front of the obduction zone. As such, Rovinj-1 bauxite and accompanying bauxite bodies belong to the 2nd type "bauxites formed in passive plate interior under intraplate stress" sensu D'ARGENIO & MINDSZENTY (1995).

Geological setting

The Rovinj-1 bauxite formed during the early Kimmeridgian to late Tithonian subaerial exposure phase, which separates the first, early Bathonian to early Kimmeridgian megasequence and the second, late Tithonian to early/late Aptian megasequence. More precisely, it is situated between the Oxfordian to lower Kimmeridgian Muča and Lim units of the first megasequence, and lower Tithonian Kirmenjak unit of the second megasequence. The Muča unit mainly comprises ooid grainstones and ooid rudstones deposited in high-energy tidal bar facies, and peloidal to skeletal wackestones deposited in low-energy conditions in the shallow subtidal. The Muča unit appears as lenses in the beds of the Lim unit, which is composed of peloidal packestones deposited in a low-energy lagoonal environment within the shallow subtidal (VELIĆ & TIŠLJAR, 1988, and references therein). The fossil assemblage of both the Muča and Lim units indicates their Oxfordian to lower Kimmeridgian age. The formation of Rovinj breccias (VELIĆ & TIŠLJAR, 1988) followed the deposition of these two units, which have formed during the regression that preceded the subaerial exposure. They show a gradual transition from Lim and Muča units and are composed from fragments of these two units. The subaerial exposure phase that followed is marked with the formation of bauxites (ŠINKOVEC, 1974; VELIĆ & TIŠLJAR, 1988) showing an erosional contact with the Lim and Muča unit, as well as the Rovinj breccias (VELIĆ & TIŠLJAR, 1988). Besides the formation of bauxites, the unconformity is also recorded as simple erosional gaps between the Muča and Lim units and the Kirmenjak unit on some localities (VLAHOVIĆ et al., 2003) as well as the deposition of palaeosols (VELIĆ & TIŠLJAR, 1988; VLAHOVIĆ et al., 2003). The end of the subaerial exposure phase is followed by the oscillating

transgression, after which the deposition of the Kirmenjak unit had begun. This unit is composed of the cyclical alternation of mudstones, mudstones with indications of subaerial exposure and finally the lenses or intercalations of black pebble breccias (TIŠLJAR, 1986; VELIĆ & TIŠLJAR, 1988). In the Rovinj-1 deposit, the immediate cover consists of a cyclic alternation of clays, brackish to marine limestones and black pebble breccias, which gradually alternate in the lower part of the Kirmenjak unit.

Provenance of the Rovinj-1 bauxite

The source material from which the Rovinj bauxite was formed, was derived from several sources, mainly from the wind-blown material and the insoluble residue, as proposed by ŠINKOVEC (1974). Volcanic material likely represented the majority of the aeolian input, which is also evident from the presence of zircon and apatite grains in the bauxite (ŠINKOVEC, 1974). The presence of multiple levels of tuffs and bentonites of Kimmeridgian age in the Trento plateau, Northeastern Italy (PELLENARD et al., 2013) and of Kimmeridgian–Tithonian age in Gorski Kotar area, central Croatia (ŠĆAVNIČAR & NIKLER, 1976; VELIĆ et al., 2002), is indicative of deposition of such materials on the area of the Adriatic Carbonate Platform during the duration of the subaerial exposure in Istria. Limestones of the Muča unit which represent the bedrock of Rovinj-1 bauxite deposit contain a relatively high content of insoluble residue (2.19%; DURN et al., 1999). During the karstification of these limestones, this material was also accumulated in karstic depressions, and subjected to bauxitisation together with wind-blown volcanic material.

Petrology, mineralogy and geochemistry of the Rovinj-1 bauxite

In the Rovinj-1 deposit, the bauxite consists mainly of red bauxite (Fig. 3a–d), while white and grey bauxite occur in the uppermost section of the deposit (Fig. 3b, c).

Red bauxite consists mainly of boehmite, haematite and anatase, with minor amounts of chlorite, rutile, and locally gibbsite (Fig. 4a). The bauxite shows a uniform mineralogical composition throughout the profile (Fig. 4a), which is in accordance with major oxide data (Fig. 4b) as they are also uniform, and do not show any significant trends throughout the profile. Grey bauxite formed during the initial flooding of the bauxite, which led to the formation of a swampy environment on top of the bauxite. The microbial activity in the swamp led to the depletion of oxygen and production of hydrogen sulphide, which in turn caused the solubilisation of iron oxides and pyritization of the topmost section of the underlying bauxite. Precipitated

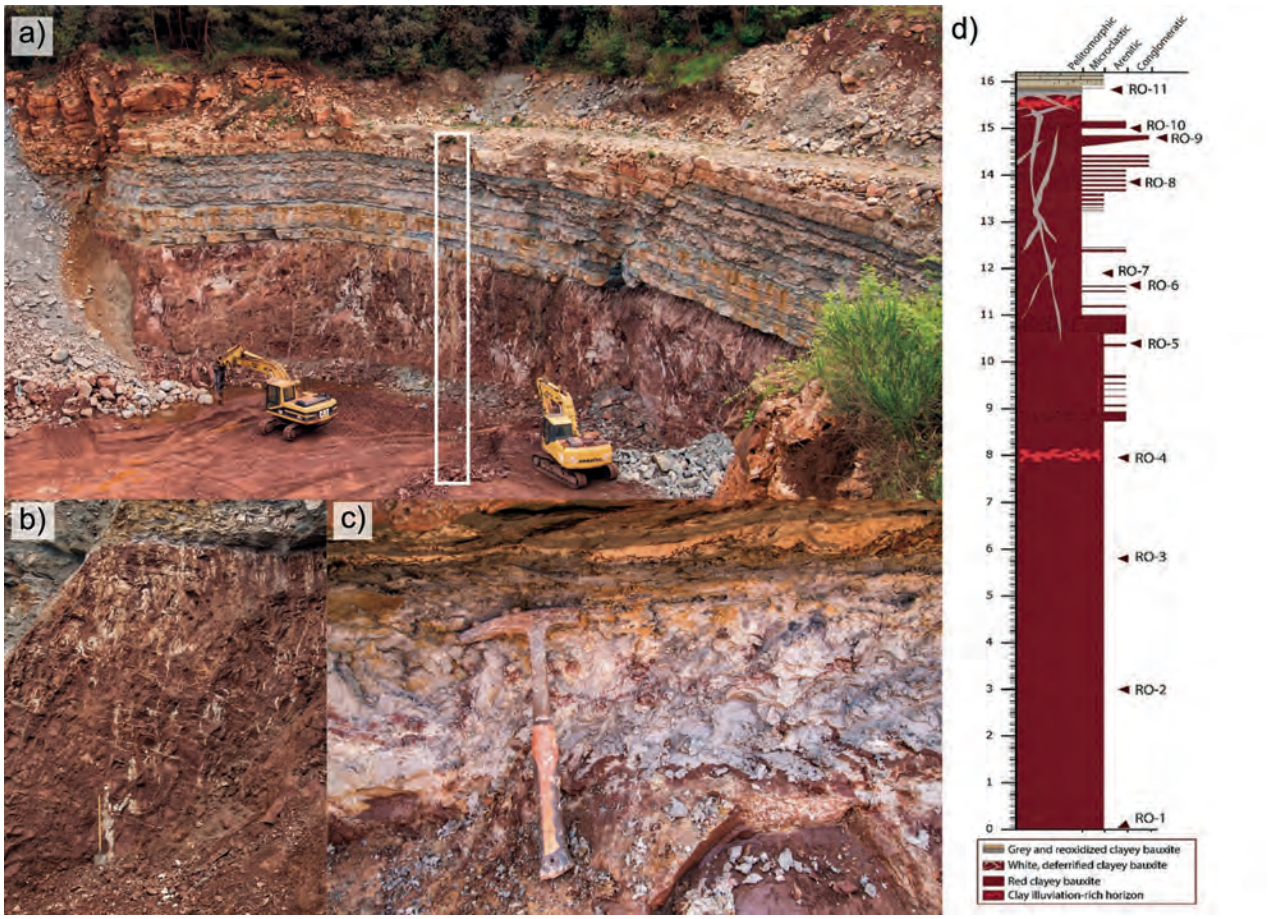

Fig. 3. Field photographs from the Rovinj-1 deposit and the analysed bauxite profile. (a) Rovinj-1 deposit with indicated position of the analysed profile. (b) Red bauxite cross-cut with veins of white bauxite. (c) Topmost part of the bauxite, with visible grey bauxite, pyritised roots and kaolinitic marl (white intercalations in the clay at the top of the photograph) and red bauxite with occurrences of white bauxite. (d) Reconstruction of the sampled bauxite profile (RO – sampling site).

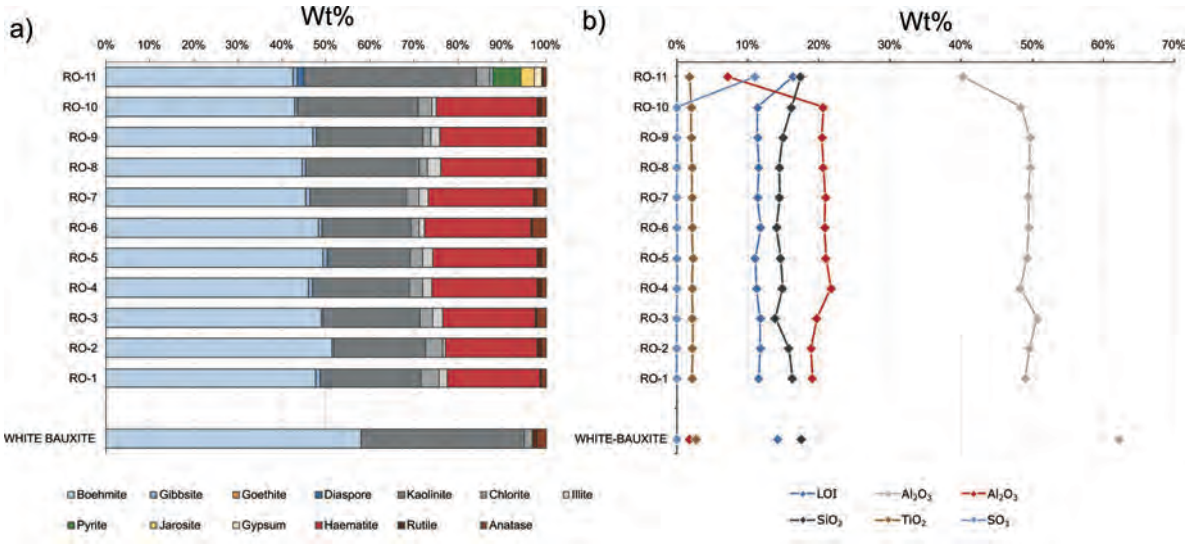

Fig. 4. Plots displaying mineralogical and chemical composition of the analysed bauxite. (a) Bulk mineralogical composition throughout the Rovinj-1 bauxite deposit. (b) Distribution of major oxides along the studied bauxite profile.

iron sulphides are present as framboids and crystals dispersed in the bauxite matrix and in the in situ pyritised root remains. As such, the grey bauxite has a similar composition as the red bauxite, but with the substitution of haematite with iron sulphides, coupled with different sulphate minerals which formed during pyrite decomposition. The major oxide content of the grey bauxite is in accordance with mineralogical content of the bauxite (Fig. 4a, b), as the presence of pyrite and sulphate minerals is also confirmed with elevated SO_3 values (Fig. 4b). White bauxite appears directly under the grey bauxite, as a metre-thick zone crosscut by the veins of the white bauxite (Fig. 3c). On closer inspection, these white bauxite veins reveal roots that have penetrated the upper part of the bauxite, which is also evident from the sporadic presence of pyritised root remains within the white bauxite veins (Fig. 3c). White bauxite is also present below this zone, extending along fractures and faults up to ten metres into the red bauxite (Fig. 3b). The white bauxite in this zone probably originated from reducing and acidic pore water that seeped into the bauxite along the fractures. Since the white bauxite is simply the deferrified red bauxite, it has the same composition but does not contain iron minerals (Fig. 4a). The concentrations of major oxides (Fig. 4b) in the white bauxite agree well with the mineralogical content (Fig. 4a), as the values for Al_2O_3, SiO_2 and TiO_2 are elevated compared to the red bauxite, while Fe_2O_3 is almost zero.

The bauxite is structurally heterogeneous, as parts of the analysed bauxite profile are mainly pelitomorphic to microclastic (Fig. 5a), with intercalations of arenitic (Fig. 5b) and conglomeratic bauxite (Fig. 5c). On the studied profile, a coarsening upward trend can be observed, as the conglomeratic and arenitic bauxite are progressively more abundant in the upper part of the profile (Fig. 3d). This may be associated with the progressive aridification of the climate in the middle Tithonian (WIGNALL & RUFFELL, 1990; RUFFELL & RAWSON, 1994; BRIGAUD et al., 2008; HESSELBO et al., 2009) as this probably led to a decrease in vegetation cover over the deposit, allowing greater erosion of the bauxite during the formation of its uppermost part.

The bauxite cover sequence

The cover sequence of the Rovinj-1 bauxite begins with the deposition of grey kaolinitic clay (Fig. 3c), which is then covered with a cyclically alternating sequence of clays, marls, limestones and black pebble breccias (Fig. 6a, b).

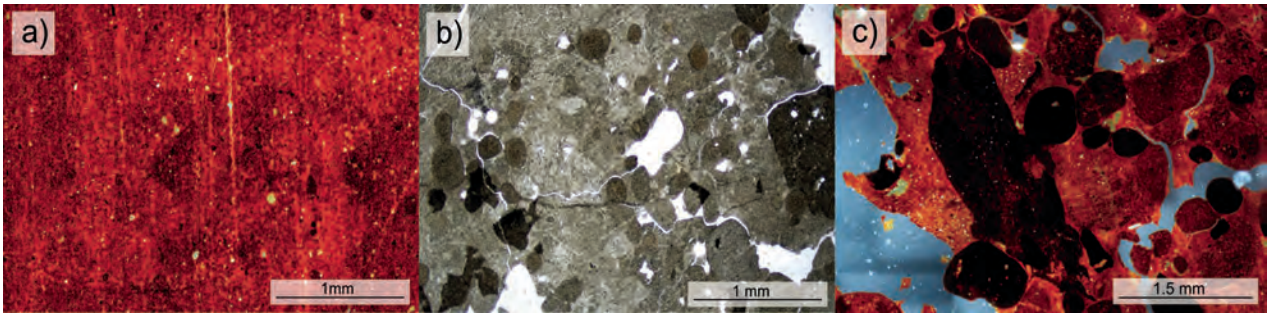

Fig. 5. Photomicrographs of different bauxite samples. (a) Pelitomorphic to microclastic red bauxite sample (RO-6), taken under conoscopic illumination. (b) White bauxite sample (RO-45) with visible arenitic structure, PPL. (c) Red bauxite sample (RO-9) with visible conglomeratic structure and bauxite clasts enriched in iron oxides, taken under conoscopic illumination.

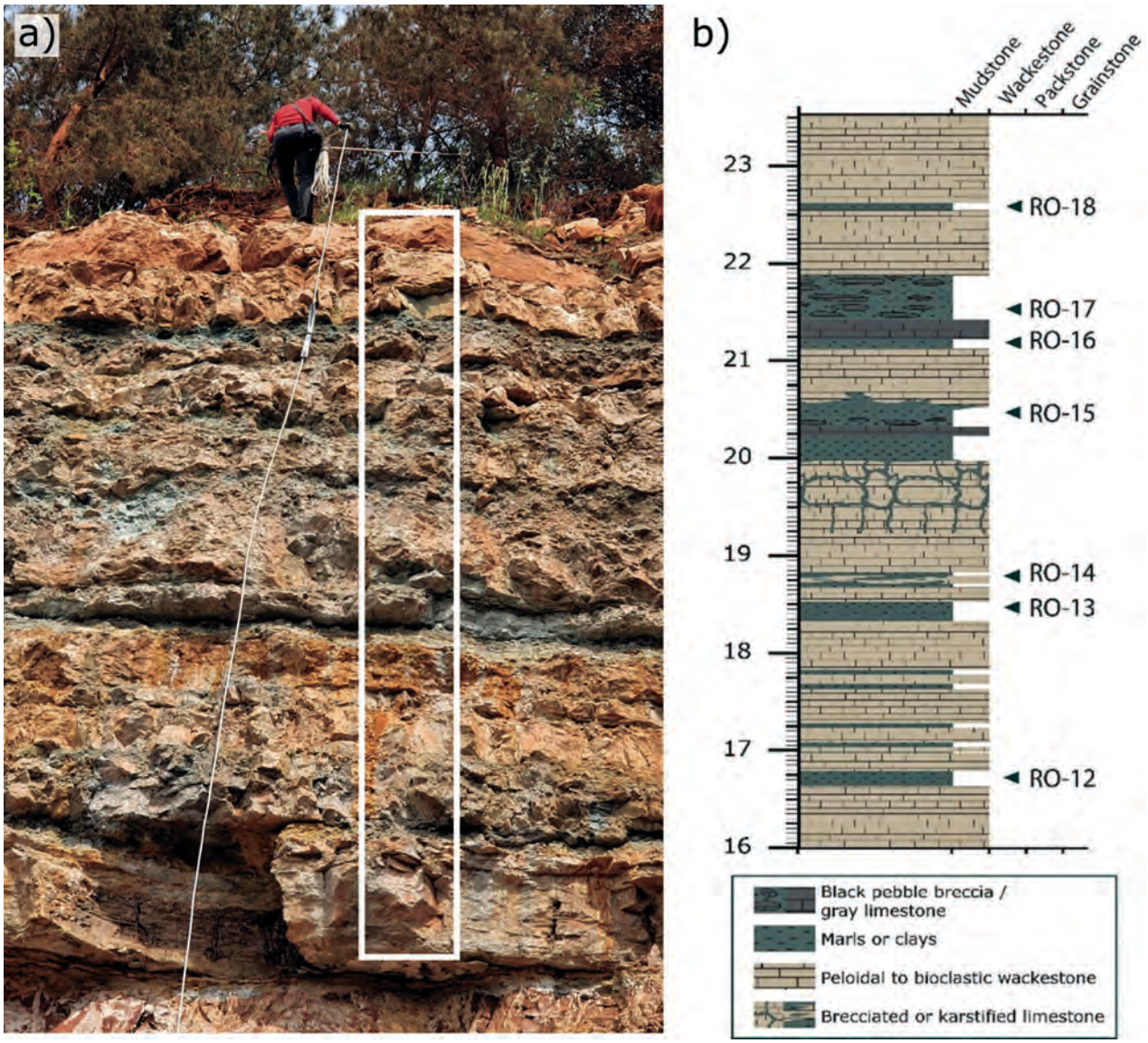

Fig. 6. Studied profile of the bauxite cover. (a) Field photograph of the profile, with the studied section indicated with the white rectangle. (b) Reconstruction of the studied cover section. RO – sampling site.

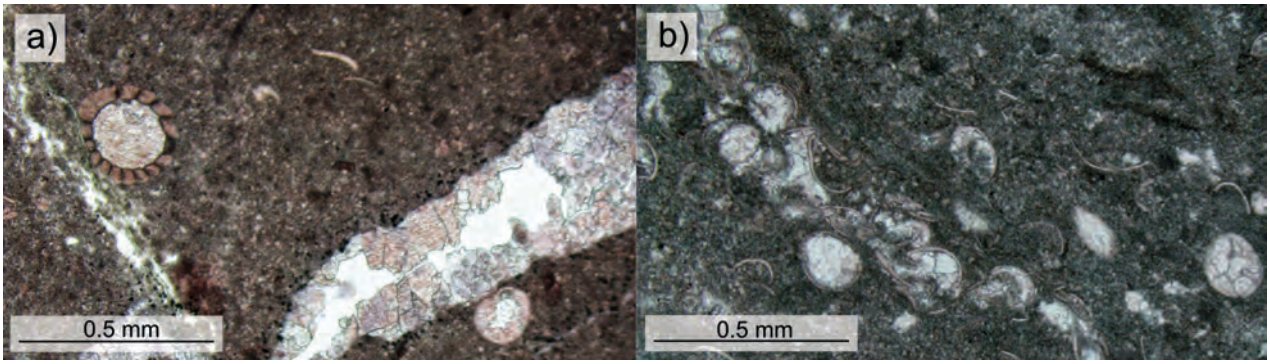

Fig. 7. Photomicrographs from the limestones in the cover sequence. (a) Charophyta oogonium, PPL. (b) Accumulation of ostracod shells, PPL.

The limestones from the cover sequence formed in a restricted environment with a very scarce fossil record, consisting exclusively of *Charophyta* oogoniums (Fig. 7a) and ostracods (Fig. 7b). Based on the aforementioned faunal and floral record, these limestones formed in conditions of fluctuating salinity (schizohaline), before they were covered with fully marine limestones of the Kirmenjak unit.

Such variations in salinity and the very restricted fauna dominated by ostracods indicate that these limestones were deposited in an isolated body of water that probably developed over the bauxite and other karst depressions

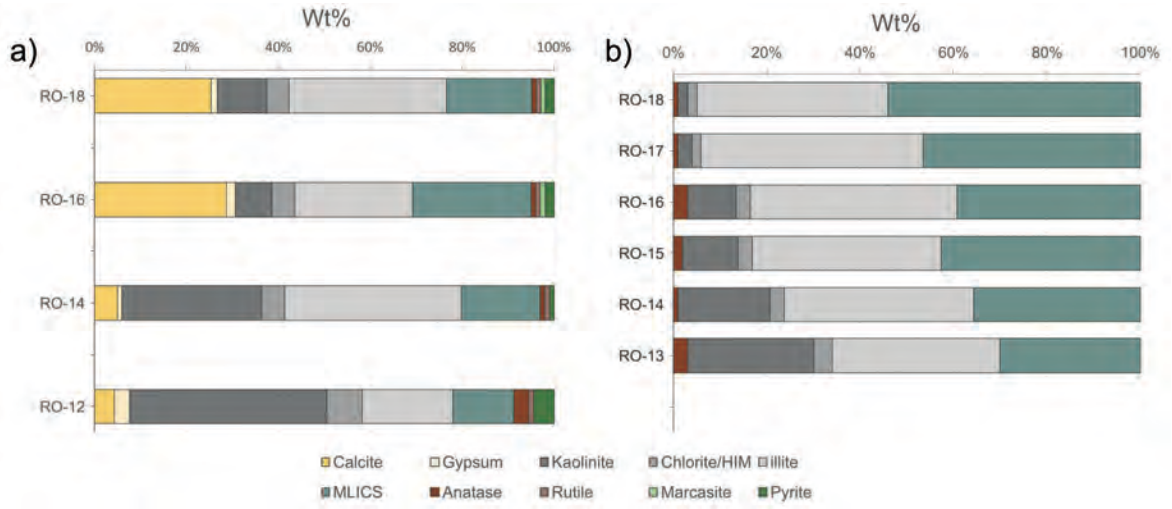

Fig. 8. Mineralogical composition of the studied clay/marl samples throughout the studied section of the Rovinj-1 bauxite deposit. (a) Bulk mineralogical composition throughout the analysed profile. (b) Mineralogical composition of the clay fraction throughout the analysed profile.

during the rise of the water table before the emerged terrain was completely flooded and the fully marine Kirmenjak unit was deposited. Such a deposition sequence is commonly referred to as a "blue hole sequence" according to RASMUSSEN & NEUMANN (1988), and is indicative of internal transgression.

Mineralogy of the cover sequence

These materials consist mainly of clay minerals (kaolinite, chlorite/hydroxyl interlayered mineral (HIM), illite, mixed layered illite–chlorite–smectite (MLICS)), calcite, and gypsum, with minor amounts of titanium oxides (rutile and anatase) and iron sulphides (pyrite and marcasite, Fig. 8a). The clay fraction has a similar composition to the bulk samples and consists of MLICS, chlorite/HIM, illite, kaolinite and minor amount of anatase (Fig. 8b). There is a gradual increase in MLICS and illite and a gradual decrease in kaolinite throughout the studied profile, best visible in the composition of the clay fraction.

This trend probably reflects aridification at the end of the Tithonian, which is also recorded in the clay record (WIGNALL & RUFFELL, 1990; HESSELBO et al., 2009) and by stable isotope data from oyster shells (BRIGAUD et al., 2008). Because the areas around the "blue hole" above the bauxite were still emerged during the initial stages of transgression, pedogenesis was not yet complete and the newly formed soils may have responded to climate change. These newly formed soils, rich in illite and mixed layered clays, gradually replaced the previously formed ferralitic soils, as indicated by the changes in clay mineralogy in the studied profile.

STOP 2 – KANFANAR QUARRY: UPPER APTIAN–UPPER ALBIAN UNCONFORMITY

The upper Aptian–upper Albian unconformity marks the division between the second, late Tithonian–early/late Aptian megasequence, characterised by facies heterogeneity and considerable thickness, and the third, late Albian–late Santonian megasequence, which is more than 1000 m thick with different facies successions (Fig. 1). Deposition of the second megasequence started at the end of the Tithonian with an oscillating transgression resulting mainly in peritidal shallowing-upward cycles. The megasequence is capped by the upper Aptian deposits, which experienced a relatively rapid shallowing, resulting in subaerial exposure (VELIĆ et al., 1989, 2003). This regional event was a consequence of a relative sea-level fall caused by the interaction of eustatic changes and synsedimentary tectonics in the Istrian part of the Adriatic Carbonate Platform (AdCP), resulting in variable duration of shallow-water conditions in different parts of the platform, as well as in varying intensity of erosion of Aptian and Barremian deposits (VELIĆ et al., 1989, 2003). The end of this megasequence was marked by deposition of breccias and conglomerates with common blackened pebbles, representing swamp conditions, interbedded with clay layers.

Terrestrial deposits associated with this regional unconformity can be found at various places (Fig. 9) such as Tri jezerca quarry, Selina 4 quarry, Balle quarry, Kanfanar quarry, Lakovići quarry, Goda quarry as well as at the road cut of 'Istrian Y' highway (OTTNER, 1999; DURN et al., 2003, 2006; MILEUSNIĆ, 2007). The duration of the stratigraphic hiatus varied between 11 and 19 million years, depending on the palaeogeographical position of individual localities (VELIĆ et al., 1989). The evidence of exposure is characterised by greenish-grey clay, found mainly in paleokarst pits, varying in thickness from a few centimetres to a meter, and coarse brecciated regolith.

Following an extensive subaerial exposure during the late Aptian and early Albian, a gradual transgression took place during the middle Albian, which eventually transitioned into a complete transgression. It marks the beginning of the third megasequence, that comprises several lithostratigraphic units (VELIĆ et al., 1995), including records of a peritidal and foreshore sedimentary system

Fig. 9. Outcrops of terrestrial deposits associated with second regional unconformity. (a) Selina quarry; (b) Kanfanar quarry; (c) Lakovići quarry; (d) Goda quarry; (e) Tri jezerca quarry; (f) Road cut of 'Istrian Y' highway near Kanfanar.

in the middle and late Albian, differentiation of sedimentary systems during the latest Albian and Cenomanian, drowned platform systems during the latest Cenomanian and Turonian (JENKYNS, 1991; GUŠIĆ & JELASKA, 1993; VLAHOVIĆ et al., 2005), and re-establishment of the shallow-water sedimentary system during the late Turonian, Coniacian and Santonian (VELIĆ et al., 2003; VLAHOVIĆ et al., 2005).

Location

For presentation of the upper Aptian–upper Albian unconformity, the studied geological profile located at the southeastern part of the Kanfanar quarry (Fig. 9c) is selected.

Kanfanar quarry is located 2 km west of Kanfanar on both sides of the road connecting Kanfanar and Rovinj. It is renowned for containing the high-quality natural stone, a light brown lower Aptian oncoid limestone, the most famous architectural and building stone from Istria, known on the market under the names *Kanfanar*, *Bale* (*Valle*), *Rose Karst* and under the general name *Istrian yellow* (*Giallo d'Istria*). The first notes on the exploitation of this stone date back to the 15th century, when it was transported from Brijuni archipelago (island of St. Jerolim) to Ancona on the order of the famous sculptor and architect Juraj Dalmatinac. The Kanfanar quarry was opened for the needs of the Austro-Hungarian railways. Since 1961, the quarry has been part of the company Kamen d. d. Pazin, and it is still active today. The extraction of the stone from the quarry employs both surface and underground methods. Some of the most famous architectural structures made of this stone are interior of the Austrian Parliament building in Vienna (Austria), Park at Krasnodar Stadium (Russia), Europa-park Colosseo in Freiburg (Germany) and Szent Istvan Szobor square in Budapest (Hungary).

Lithology, sedimentology and micropaleontology of carbonates

A total thickness of 20.85 m (9.60 m below and 11.25 m above the unconformity; Fig. 10) of predominantly shallow-water platform carbonates comprising the second unconformity was examined to: (1) reconstruct environmental changes around the unconformity in more details, (2) refine/define lithostratigraphic subdivision of the Aptian and Albian deposits and (3) define extensive subaerial exposure phase – regional unconformity during the late Aptian and early Albian. The focus was on the shallow-water carbonates deposited in inner-platform peritidal environments overlain by carbonate breccia with clayey calcareous matrix and greenish-grey clay, both marking a regional unconformity, and on the succession on its top (Fig. 10). The lithology, sedimentology and microfossil content of the studied section were analysed and described on site at cm-scale.

Fig. 10. Kanfanar quarry. (a) Kanfanar section below unconformity level; (b) and (c) Section including regional unconformity and succession above it.

A total of 71 samples were collected for sedimentary (petrographic) and micropalaeontological analyses. Benthic foraminifera together with other biogenic and lithologic constituents are used to reconstruct sedimentary environments and conditions that existed during depositional history of the investigated Lower Cretaceous succession in western Istria (CVETKO TEŠOVIĆ et al., 2011).

Based on lithological features and micro- and macrofossil assemblages, seven lithofacies types (LF1–LF7) were determined (Fig. 11, Tab. 1).

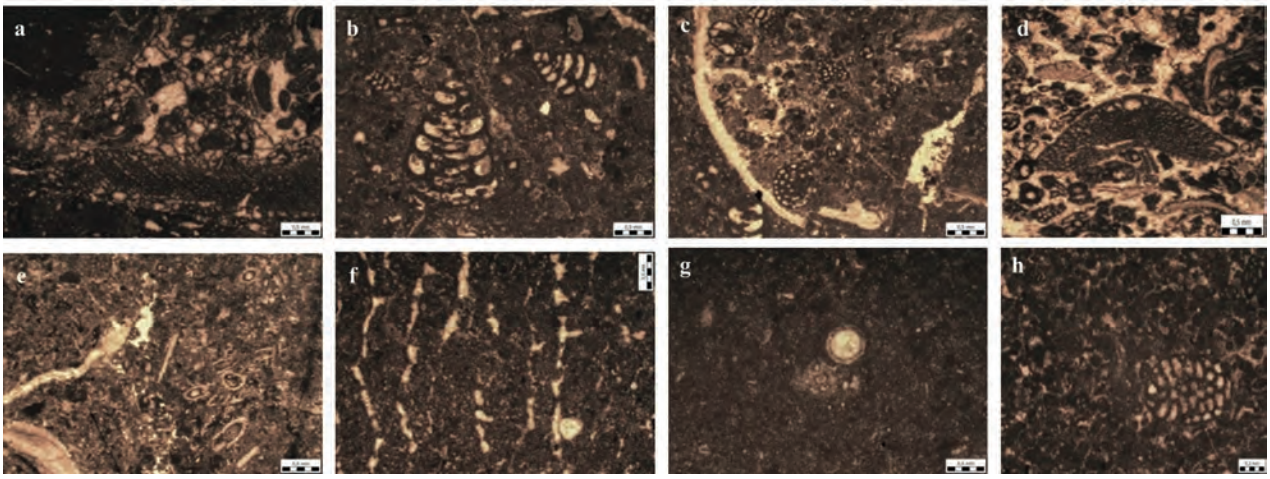

Fig. 11. (a) Bacinella wackestone–floatstone: *Palorbitolina lenticularis* (BLUMENBACH), *Bacinella irregularis* RADOIČIĆ (LF1, KA-1). (b) Foraminiferal-peloidal wackestone–packstone: *Praechrysalidina infracretacea* LUPERTO SINNI (LF2, KA-8). (c) Foraminiferal-peloidal packstone: *Voloshinoides murgensis* LUPERTO SINNI and MASSE, *Archaealveolina reicheli* (DE CASTRO), (LF2, KA-8). (d) Peloidal-bioclastic packstone–grainstone: *Palorbitolina lenticularis* (BLUMENBACH) (LF3, KA-24). (e) *Decastronema*-algal packstone: *Salpingoporella dinarica* RADOIČIĆ (LF4, KA-28;). (f) Fenestral-peloidal wackestone–packstone (LF5, KAK-10A). (g) Characean-ostracod wackestone (LF6, KAK-24;). (h) Peloidal-miliolidal packstone: "*Valdanchella*" *dercourti* DECROUEZ and MOULADE (LF7, KAK-27).

Tab. 1. Kanfanar lithofacies types (LF) with texture, sedimentary structures, skeletal and not-skeletal particles, and depositional environment.

Kanfanar lithofacies (LF)		Texture, sedimentary structures, skeletal and non-skeletal particles	Depositional environment
LF1	**Micritic limestones with *Bacinella* oncoids and low diversity biota**	Wackestone–floatstone with *Bacinella* oncolites and common bioturbated features. Benthic foraminifera (common **orbitolinids** – *Palorbitolina lenticularis*), **bioclasts** of bivalve fragments (mostly requiniid rudists –shells of *Toucasia* sp.)	Lagoons and low-energy shallows with a very low sedimentation rate, common bioturbated levels, and low biotic diversity
LF2	**Finer-grained micritic limestones**	Mostly wackestone–packstone with intraclasts, bioclasts, peloids, benthic foraminifera and bivalve shells.	Subtidal environment of elevated water energy to moderate energy
LF3	**Grainy limestones with diverse biota**	Foraminiferal-peloidal packstone–grainstone with more diverse biota: common benthic foraminifera (*Palorbitolina lenticularis*), decastronemas, bivalve and echinoderm fragments and occasionally dasycladal algae (predominate *Salpingoporella dinarica*).	Deepening of the sedimentary environment and deposition in somewhat deeper subtidal environments characterised by higher biotic diversity
LF4	***Decastronema*-algal limestones**	Wackestone and wackestone–packstone. Abundant dasycladal algae – *Salpingoprella dinarica, rare Decastronema*? and benthic foraminifera and thaumatoporellaceans. Less common fragments of rudists and other bivalve shells. Common small peloids.	Restricted to open shallow subtidal carbonate platform with moderate water energy
LF5	**Fenestral micritic limestones occasionaly laminated with very low diversity biota**	Mudstone–wackestone, locally packstone, with peloids, ostracods shells, algal filaments, pedoturbations, desiccation cracks and circumgranular cracks. Rare *Decastronema*?, thaumatoporellaceans, nubeculariids and sporadically common miliolids.	Restricted and protected shallow subtidal and intertidal inner carbonate platform with low water energy
LF6	**Micrites with ostracods and characean remains**	Wackestone with numerous ostracod shells, rare characean oogonia and algal filaments, gastropods and thaumatoporellaceans. Locally laminated.	Shallow subtidal carbonate platform with low water energy (with occasional fresh water influence)
LF7	**Fine-grained limestones with abundant miliolids**	Wackestone–packstone and packstone–grainstone with abundant miliolid and other benthic foraminifera, micritized gastropod fragments. Less common intraclasts, peloids and rare aggregated grains.	Shallow subtidal carbonate platform with moderate water energy

Mineralogy and micromorphology of greenish-grey clay

In the Kanfanar area, the subaerial exposure phase which commenced during the late Aptian left clay deposit up to 40 cm thick. Within the transgressive upper Albian deposits which overlain clay deposit, features suggesting multiple brief subaerial exposures events are recorded, primarily manifested through coarse brecciated zones filled with greenish-grey and greenish-yellow clay.

Four samples of the 40-cm-thick greenish-grey clay (5GY6/1 to 5GY7/1 after Munsell) in the central part of the quarry outcrop were collected along the profile (Fig. 12) for various analyses, including mineralogical, chemical and micromorphological analyses. Samples of carbonates situated immediately below the clay were also collected and analysed.

The greenish-grey clay does not exhibit significant variation in colour, microstructure and fabric along the profile. The samples are grey with areas of yellowish and greenish hues, and the microstructure is predominantly granular, angular blocky, and planar (Fig. 13a, b, c). The yellowish patches are partially opaque and likely composed of iron oxides (Fig. 13e). Pyrite sporadically appears in aggregates of typical nodules (Fig. 13g) and framboids.

The birefringent fabric of the micromass (b-fabric) also shows little variation, with random streaking, stipple-speckled b-fabric (Fig. 13d, f), cross-streaking, and

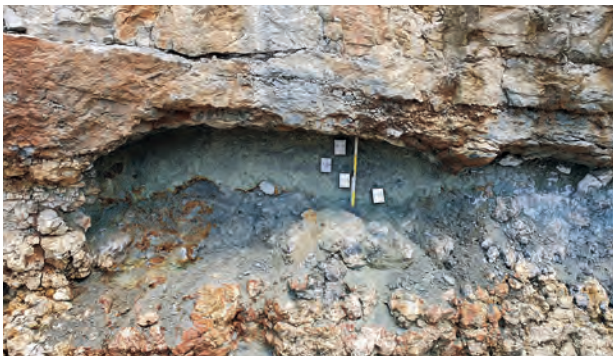

Fig. 12. Profile of greenish-gray clay in the Kanfanar quarry with Kubiena boxes for micromorphological analyses

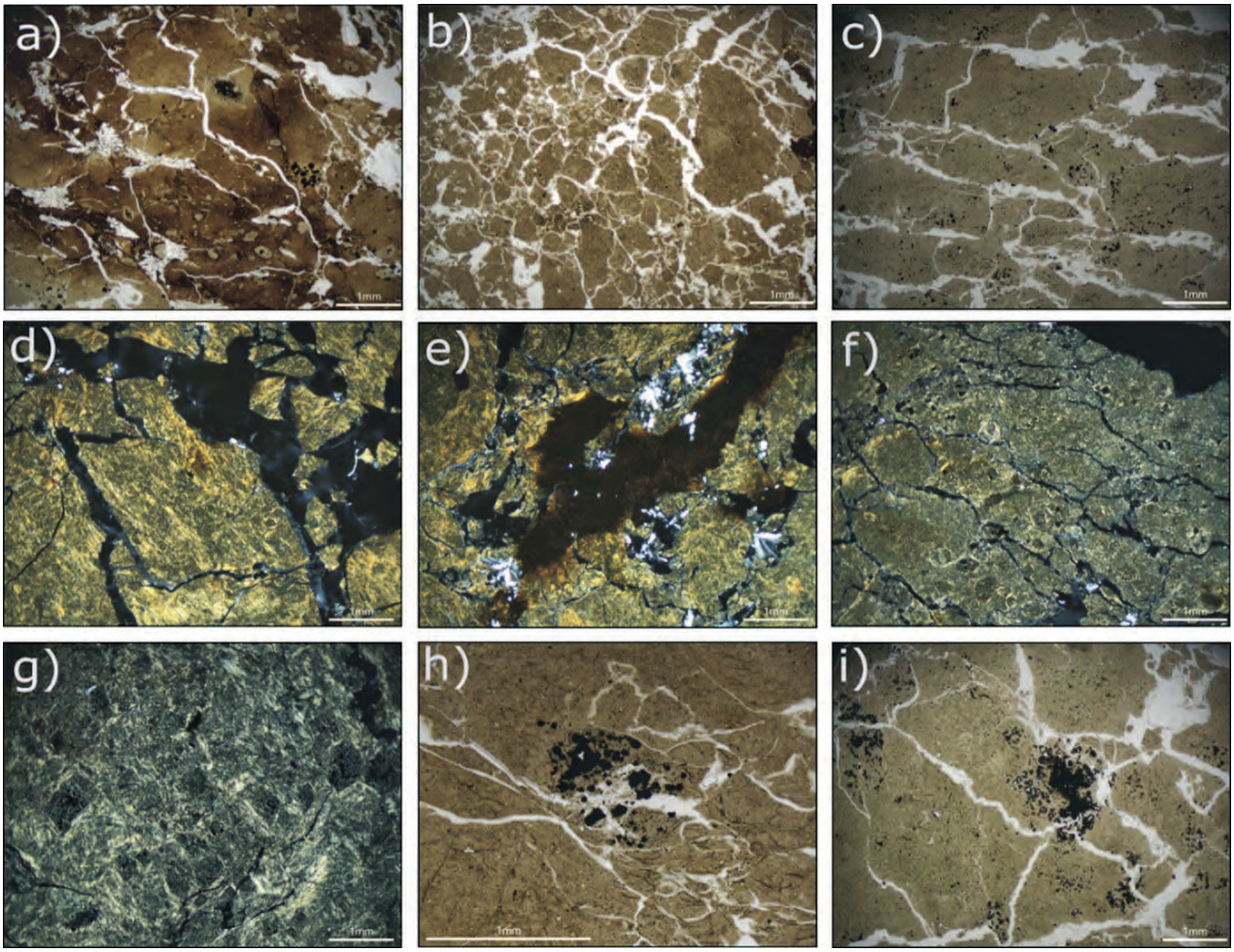

Fig. 13. Photomicrographs of greenish-grey clay from the Kanfanar profile. (a) Subangular blocky microstructure with visible gypsum rosettes and impregnation of peds with iron oxides – K-1. (b) Complex microstructure consisting of granular, channel, and subangular blocky microstructure – K-1M2. (c) Subangular blocky to planar microstructure – K-2. (d) Parallel striation and stipple-speckled b-fabric (photograph taken under crossed polarised light) – K-4. (e) Impregnation of iron oxides with the appearance of gypsum rosettes (photograph taken under crossed polarised light) – K-4. (f) Clearly visible granostriation and stipple-speckled b-fabric (photograph taken under crossed polarised light) – K-1M2. (g) Granostriation around clasts rich in typical orthic nodules of pyrite and clearly visible cross-striation of b-fabric (photograph taken under crossed polarised light) – K-3. (h) Clast rich in typical orthic nodules of pyrite – K-3. (i) Aggregated typical orthic nodules of pyrite – K-2.

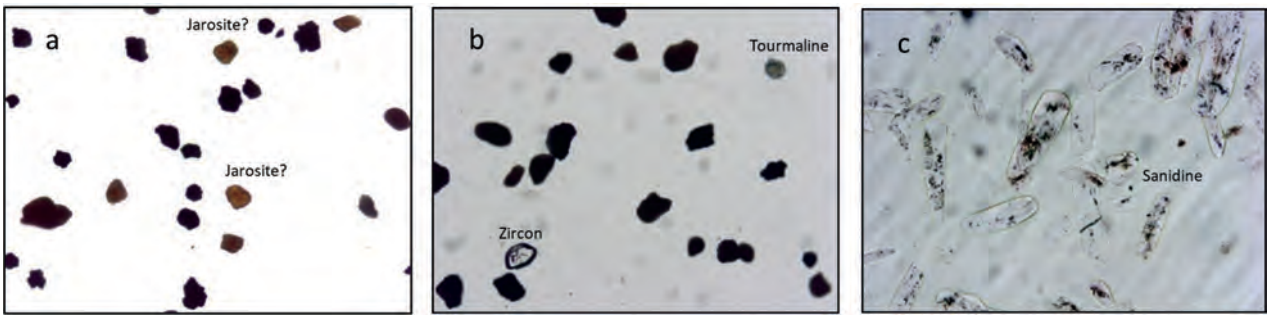

Fig. 14. Photomicrographs of greenish-grey clays – heavy (a and b) and light mineral fraction (c) from the upper part (0–20 cm) of the Kanfanar greenish-grey clay profile

granostriated b-fabric (Fig. 13h, i) alternating throughout the sample.

Based on X-ray diffraction, the greenish-grey clays consist mainly of phyllosilicates (60–90 wt%), followed by K-feldspar (5–10 wt%), gypsum (5–10 wt%), quartz (up to 5 wt%) and a mineral from the Ti-oxide group (anatase, up to 2 wt%). Iron sulphide (pyrite, 2–4 wt%) and sulphate (jarosite, 2–8 wt%) are also observed. It is possible that altered plagioclase – albite – may be present in the analysed samples, but this could not be confirmed with certainty. Phyllosilicates are represented by micaceous (illitic) material (35–40 wt%), followed by illite–smectite (15–45 wt%) of variable composition which occurs in several phases (determined by the ratio of its illitic and smectitic components) and discrete smectite from the dioctahedral montmorillonite–beidellite series (5–7 wt%). Quantification did not account for the amorphous component, the content of which, based on the shape of the central portion of the diffraction curves, is estimated to be between 5–10 wt%. Given the low carbon content, it is most likely associated with poorly crystalline oxy-hydroxides or potentially volcanic glass. The distribution of clay minerals does not exhibit a clear trend along the profile. The insoluble residue of limestone beneath the greenish-grey clay consists mainly of smectite, and also contains illite and kaolinite but no mixed-layered minerals. Of the non-clay minerals, it contains a small amount of goethite (up to 5 wt%).

Heavy mineral fraction (size fraction 32–125 microns) is dominated by opaque minerals, most likely pyrite and jarosite, but also contain zircon and tourmaline (Fig. 14a, b). Light mineral fraction consists almost exclusively of bright anhedral sanidine (Fig. 14c).

Interpretation

During the early Aptian in the area of the Adriatic Carbonate Platform spacious lagoons and low-energy shallows were formed characterised by a very low sedimentation rate. Consequence is the thin succession deposited in a relatively long early Aptian period with common bioturbated levels. During this transgressive phase, the deepening of the sedimentary environment and the deposition in somewhat deeper subtidal environments was characterised by higher biotic diversity (dominated by orbitolinid foraminifera) as a consequence of the relative sea-level rise and ecological disturbances, probably eutrophication caused by an oceanic anoxic event. The lower Aptian deposits represent a regionally recognisable event related to the partial drowning of the carbonate platform, which correlates well with the early Aptian oceanic anoxic event (OAE 1a; e.g., JENKYNS, 1980; MENAGATTI et al., 1998; JONES & JENKYNS, 2001; VLAHOVIĆ et al., 2005; HUCK et al., 2010; CVETKO TEŠOVIĆ et al., 2011). The first 3–5 m of the lower Aptian succession are commonly characterised by the presence of bivalves, manly requieniid shells of *Toucasia* sp. and benthic foraminifera, as well as oncoids of *Bacinella irregularis* RADOIČIĆ. The overlying massive limestones, known as the architectural-building stone "Istrian Yellow" (for its characteristic yellowish colour), are composed of cyclical alternations of mudstones/wackestones and *Bacinella* oncoid floatstones (TIŠLJAR, 1978). The lower Aptian oncoid limestones are very variable in thickness (max. 19 m) as a consequence of different duration of the regional Aptian–Albian subaerial exposure phase in the Istrian part of the AdCP. This unconformity was caused by variable amounts of synsedimentary tectonics and erosion during the late Aptian and early Albian (VELIĆ et al., 1989; MATIČEC et al., 1996) and it is clearly visible with breccias, some conglomerates, marl and clay (Fig. 15). The Kanfanar section indicates a contact between the lower and upper Aptian deposits. Lower Aptian age is confirmed by the presence of the characteristic early Aptian taxa, including *Palorbitolina lenticularis*, whereas the latest Aptian age is suggested by common dasycladacean *Salpingoporella dinarica* and foraminifera *Praechrysalidina infracretacea* deposited in protected to agitated shoals of the carbonate platform. The shallowing tendency is indicated by laminated mudstones/wackestones with fenestral fabric overlain by breccia/conglomerate beds of the first subaerial exposure surface. The end of the deposition in western Istria is marked mainly by shallowing and a long-lasting subaerial exposure (Fig. 15).

Greenish-grey clay found in the palaeokarst depressions of the Kanfanar quarry are remnants of ancient soils that ranged from seasonally marshy to permanently waterlogged conditions. These soils were formed through the erosion and accumulation of surficial soils and sediments during a phase of oscillating marine transgression that

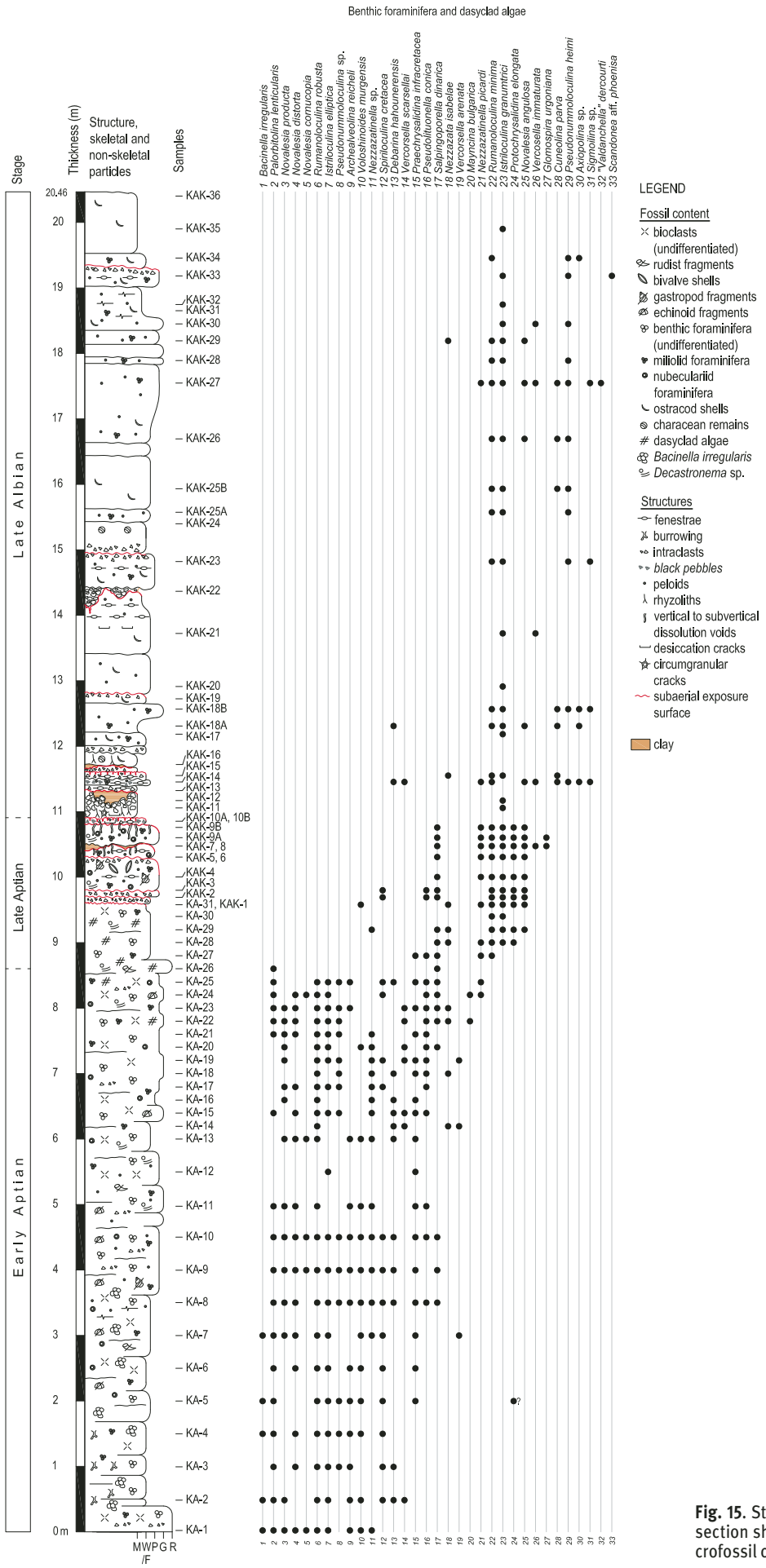

Fig. 15. Stratigraphic column of the Kanfanar section showing structures, textures and microfossil content.

marked the end of the subaerial exposure period. This interpretation has been supported by results of micromorphological analysis that showed granular, subangular blocky, and channel-like microstructures which clearly point to the reworked and bioturbated sediment. This indicates that prior to burial, the sediment was subjected to pedogenic processes over an extended period under conditions of fluctuating high-water levels. Furthermore, the granostriation around clasts (which are weakly rounded, indicating bioturbation processes or very short transportation) also effectively points to pedogenesis. The birefringent fabric of the micromass (b-fabric) shows patterns which are likely the result of various processes such as sedimentation, soil formation, and diagenesis.

Clay mineralogy do not show clear vertical trend along the Kanfanar profile, as it was found in Tri jezerca quarry where there is indication of smectite through the mixed-layered illite–smectite to illite transformation by fixation of potassium from plants, marine waters, volcanic dust and other sources through wetting and drying cycles which was supported by experiments. Deposits that bear strong sedimentological and palaeogeographical resemblance can be found in Jurassic–Cretaceous marine carbonate sequences of the Swiss and French Jura Mountains. These formations are referred to as Purbeckian sediments and have been described by DECONINCK et al. (1988).

Considering the isolation of the Adriatic Carbonate Platform during the Aptian–Albian, probably three potential source materials contributed to the formation of the greenish-grey clay related to the upper Aptian–upper Albian unconformity: (1) insoluble limestone residue; (2) aeolian dust; and (3) volcanic material. The limited presence of insoluble limestone residue, signs of vadose zone (geopetal structures, crystal silt), and shallow palaeokarstification in limestone suggests its minor contribution. Significant atmospheric circulation and accumulation of a large amount of aeolian material during Aptian and Albian due to arid climate on land and presence of metamorphic minerals (such as kyanite, garnet, staurolite, epidote and clinozoisite found in the Tri jezerca clay) indicate minor contribution of aeolian material derived from the surrounding continental blocks. Indicators such as immobile chemical element ratios, a negative europium anomaly, altered volcanic glass, and especially the abundance of bright anhedral sanidine suggest that the parent material from which the greenish-grey clays formed is largely volcanic in origin.

The late Albian microfossil assemblages from western Istria consist predominantly of the characteristic late Albian forms ("*Valdanchella*" *dercourti*, *Pseudonummoloculina heimi*, *Cuneolina parva* etc.). The low diversity assemblages without typical index fossils is probable of the late Albian age containing common miliolid forms *Istriloculina granumtrici*, *Rumanoloculina minima*, *Sigmilina* sp., *Axiopolina* sp. and less common *Scandonea* aff. *phoenissa* and *Glomospira urgoniana* (CVETKO TEŠOVIĆ et al., 2011). Depositional environments with the determined upper Albian deposits exhibit features of the so-called oscillating transgression (TIŠLJAR et al., 1995) characterised by peritidal limestones, high-energy breccias/conglomerates (e.g., the Kanfanar quarry), common laminated deposits with well-developed fenestrae and stylolites.

STOP 3 – HISTORIC BAUXITE MINE, MINJERA (THE PALAEOGENE BAUXITE-BEARING AREA OF MINJERA): UPPER CENOMANIAN/UPPER SANTONIAN–LOWER EOCENE UNCONFORMITY

The 3rd stop comprises a group of smaller Palaeogene bauxite bodies located in the valley of the Mirna river in Istria, called Minjera bauxites. Compared to other Palaeogene bauxites from Istria, they are characterised by their complete or partial reduction and subsequent pyritization. Such pyritized bauxites have been documented throughout the Jurassic and Palaeogene in the Mediterranean bauxite belt, with the best examples found in Montenegro (DRAGOVIĆ, 1989; RADUSINOVIĆ & PAPADOPOULOS, 2021), Hungary (BARDOSSY, 1982), and Greece (ECONOMOU-ELIOPOULOS et al., 2022; LASKOU & ECONOMOU-ELIOPOULOS, 2007, 2013). This pyritization phase is epigenetic in all these deposits as well as in the Minjera bauxites and is related to the transgression that succeeded the bauxitization phase. This unique grey bauxite from the Minjera locality was mined in the past for the production of alum and vitriol, which were obtained by processing pyritized bauxite. Only the grey bauxite was used as ore, while the mined non-pyritized red bauxite, which occurred in some Minjera bauxites, was left on tailing heaps in the area. Mining in Minjera probably dates back to the 16th century, but was historically documented from 1784 to 1824 (D'AMBROSI, 1926), when the mine was in operation. The Minjera bauxite deposits are of great importance as they are the first locality where bauxite was mined in the world. There are visible differences in the type of mining between the individual bauxite bodies, as many larger bauxite bodies contain adits indicating underground mining, while some of the smaller bauxites do not contain adits and were probably surface mined. Most of the deposits are present as large and sub-vertical canyon-type ore bodies (20–30 m thick), while the rest are smaller (< 5 m thick) and have mainly sinkhole morphology. The main part of the canyon-type deposits is located on the northern side of the Mirna River in this area, while the sinkhole type and smaller canyon-type deposits are found on the southern side, indicating the variability of the palaeotopography during the formation of the Minjera bauxites (Fig. 16).

Regional and geotectonic setting

Minjera bauxites are an example of the Palaeogene bauxites found throughout Istria, and their formation coincides with the widespread bauxitization event in the Perimediterranean area, during which a variety of bauxites developed, extending from Hungary through Slovenia, Croatia, Bosnia and Herzegovina, Albania and Greece. This widespread bauxitization event coincides with the Late Cretaceous closure of the Vardar Ocean (SCHMID et al., 2008, 2020; VAN HINSBERGEN et al., 2020), which

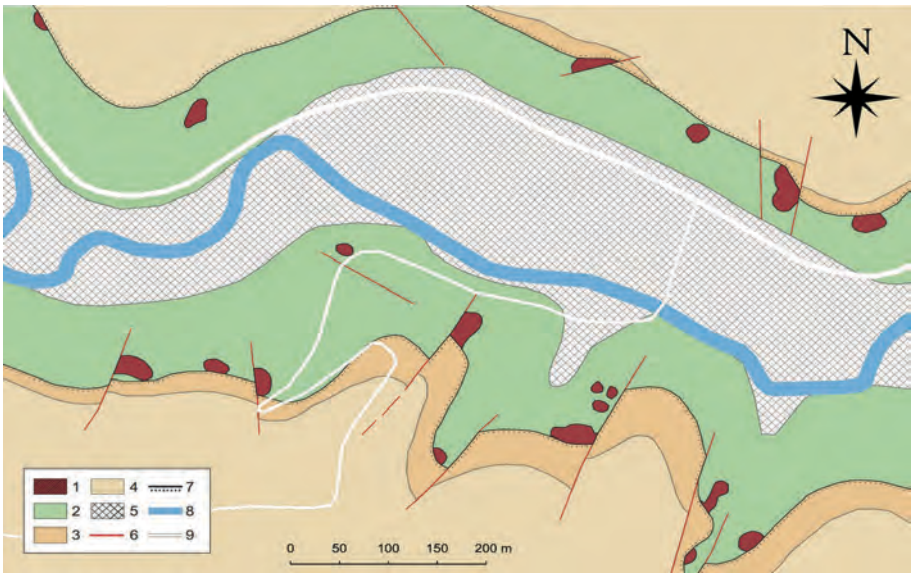

Fig. 16. Geological map of the Minjera bauxites area, modified after ŠINKOVEC et al. (1994). Legend: 1 – Bauxite; 2 – Rudist limestones; 3 – Kozina beds; 4 – Foraminiferal limestones; 5 – Quarternary aluvial deposits; 6 – Faults; 7 – Unconformity; 8 – Mirna River; 9 – Roads.

caused the formation of a foreland basin and deformation that led to the uplift of the advancing carbonate terrains and bauxitization in the emerged areas. In the area of the Adriatic Carbonate Platform the flexural foredeep formed, externally accompanied by the development of the flexural forebulge in response to the overburden pressure generated by the advancing nappes. The emerged areas in the developed flexural forebulge likely served as the environment in which the Paleogene bauxites of Istria and Dalmatia formed. As such, these bauxites belong to the 1st type – "bauxites in collisional settings" – sensu D'ARGENIO & MINDSZENTY (1995). The duration of this subaerial exposure phase was between 25 Ma (southern Istria and Mt. Učka) and 40 Ma (northern Istria). More than 10,000 bauxite occurrences and deposits are known in Istria, as an evidence of a widespread and intensive bauxitization during this period. As deformation continued, rapid subsidence and disintegration of the former Adriatic Carbonate Platform began, resulting in the temporary restoration of carbonate production in the form of foraminiferal limestones, followed by transitional beds and turbidite deposition, accumulating over the former fore-bulge and bauxites (VLAHOVIĆ et al., 2005).

Geological setting

Structurally, the Minjera bauxites are located in the northern Istrian Buzet–Savudrija brachianticline. The bauxites are located on karstified bedrock consisting of Cenomanian rudist limestones, while their hanging wall consists of brackish to freshwater limestones of Eocene age, also called Liburnian deposits or Kozina beds (ŠINKOVEC et al., 1994). During the early Cenomanian period, there were notable changes in the depositional environment in the study area. Prograding sand bar bodies with rudist and chondrodont bioclasts surrounded by peritidal lagoons with rudist biostromes were formed. Rising sea-level led to the destruction and redeposition of calcareous sand bars. Subsequently, lagoonal limestones with rudist and chondrodont coquinas and pelagic influence developed. Increased pelagic influence was observed in younger limestones, featuring calcisphaeres, silicisponge spicules, algae, and planktonic foraminifera (VLAHOVIĆ et al., 1994). Shallowing-upward sequence marks the final deposits in the middle Cenomanian, which consisted of rudist mounds and biostromes together with associated low-energy shoals. These limestones are karstified in the Mirna river valley, and overlain with numerous bauxite bodies and transgressive Palaeogene beds (VLAHOVIĆ et al., 1994). Karstification proceeded along joints intersections, developing numerous vertical sinkholes and decameter-sized karst canyons that served as sediment traps and places where bauxite may have formed and accumulated. This indicates that this carbonate terrain must have been uplifted at least several dozen metres above the sea level. The red colour and oolitic nature of the Palaeogene bauxites that developed in northern Istria are consistent with the highly elevated and intensely karstified carbonate bedrock, as such bauxites belong to the vadose lithofacies (D'ARGENIO & MINDSZENTY, 1995) typical of such terrains. Some bauxite occurrences in northern Istria, such as the Minjera bauxites, were exposed to reduced pore waters during the transgression that followed their deposition, resulting in the reduction of haematite and precipitation of iron sulphides. In some cases, entire bauxite bodies were exposed to this process, which completely transformed them into grey and pyritized bauxite, as is the case with the Minjera bauxites. The transgression was marked with the deposition of the Kozina beds, which are restricted to the immediate hanging wall of the Minjera bauxites, as they indicate deposition in freshwater and brackish ponds which developed in palaeodepressions related to the bauxite-filled sinkholes and vadose canyons. The Kozina beds in this area consist of a sequence of bituminous, gastropod-rich limestones and coal seams. Charophyta oogonies found in most layers point to the freshwater to brackish-water depositional environment, but they alternate with layers abundant in

milliolids, indicating a periodic marine influence during their deposition (ŠINKOVEC et al., 1994). The Kozina beds in this area are gradually replaced with foraminiferal limestones, indicating a gradual transition from a freshwater–brackish water environment to an open marine environment.

Mineralogy and geochemistry of the Minjera bauxites

ŠINKOVEC et al. (1994) studied the D-15 bauxite deposit in detail, while recent studies reexamined the D-15 deposit, together with the previously unanalysed D-1 deposit (Fig. 17) and red bauxite left on tailing heaps during the mining of pyritized bauxite from these deposits.

Recent studies have revealed the petrographic, mineralogical, and geochemical differences between the two bauxite bodies. Both the bauxites from D-1 and D-15 deposits originally show an oolitic structure with abundant bauxite clasts (Figs. 18a, b, c, d, e), which is not surprising since the same structure was observed in the nonpyritized red bauxite sample (Fig. 18f).

The D-15 bauxite deposit contains mainly grey bauxite composed primarily of kaolinite and moderate to high amounts of diaspore, with small to moderate amounts of boehmite and iron sulphides (Fig. 19a). Diaspore occurs as a replacement for boehmite and the clay matrix as clusters of 20–50 μm prismatic crystals as well as in veins where it is associated with iron sulphides, clearly post-dating the development of structures and minerals formed during bauxitization. The D-1 deposit consists mainly of pyrite-bearing bauxite (Fig. 18a, c, d), which is predominantly boehmite and iron sulphides (pyrite and marcasite) and contains little or no kaolinite and diaspore (Fig. 19a). Red bauxite is mineralogically most similar to the D-1 bauxites in that they both contain very little kaolinite and a high amount of boehmite, but differ in iron phases (Fig. 19a), which is related to epigenetic pyritization in the D-1 deposit. The major oxide content agrees well with the mineralogical data, as the increased kaolinite content in the D-15 deposit corresponds to higher SiO_2 values, while the increased Fe_2O_3, SO_3, and Al_2O_3 values in the D-1 deposit correspond to higher boehmite and iron sulphide content than in the D-15 deposit. During subrecent weathering of grey bauxite, pyrite was oxidised, producing sulphuric acid that reacted with the phases present in the bauxite and led to the formation of sulphate minerals such as jarosite, pickeringite, and gypsum (Fig. 19a).

The differences in bauxite quality between deposits are probably due to differences in palaeotopography and morphology of the deposits. The bauxite from deposit D-1 is mainly boehmitic and is of higher quality, which is related to the steeper morphology and larger size (> 20 m thick) of the bauxite deposit compared to deposit D-15, which is much smaller and less steep (< 5 m thick). Most of the larger canyon-type bauxite bodies such as the D-1

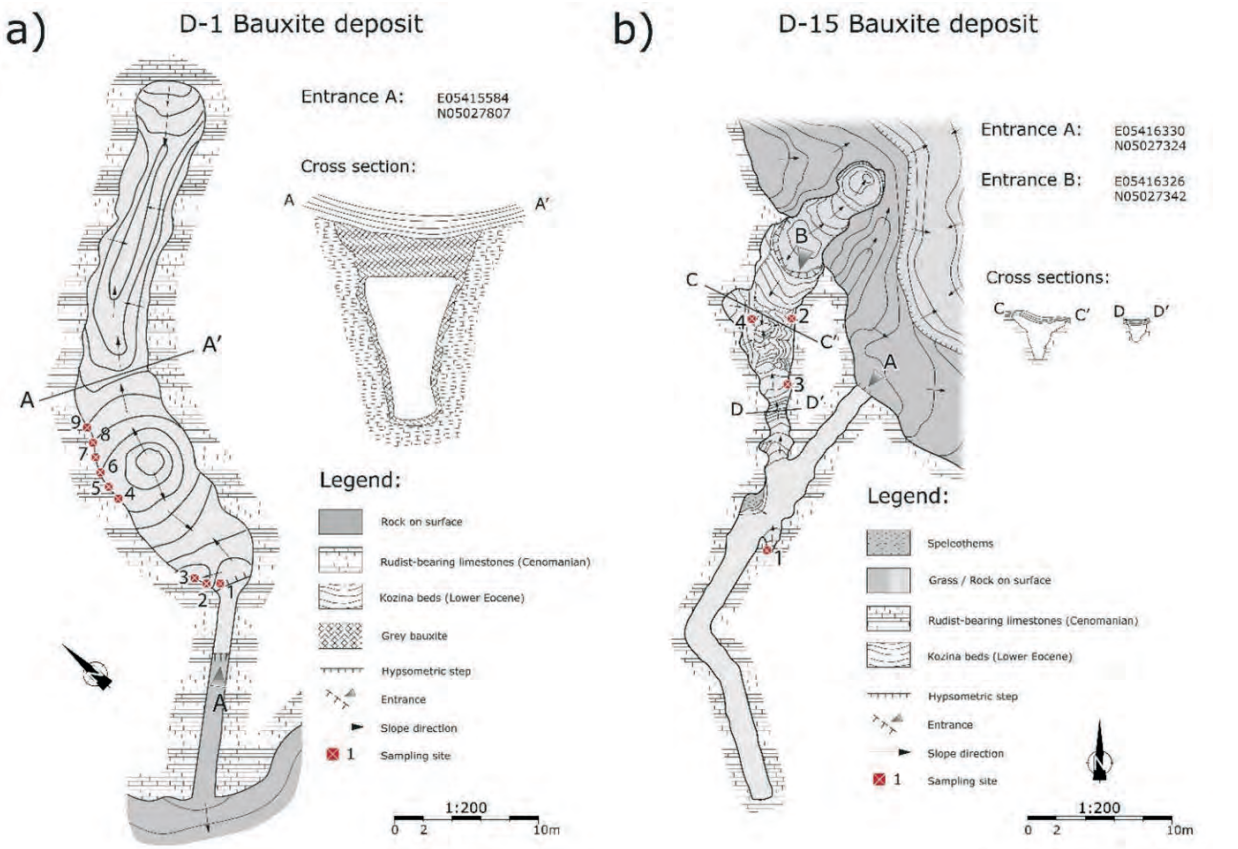

Fig. 17. Plans of the investigated Minjera bauxite deposits and the sampling sites. (a) Plan of the bauxite deposit D-15. (b) Plan of the bauxite deposit D-1.

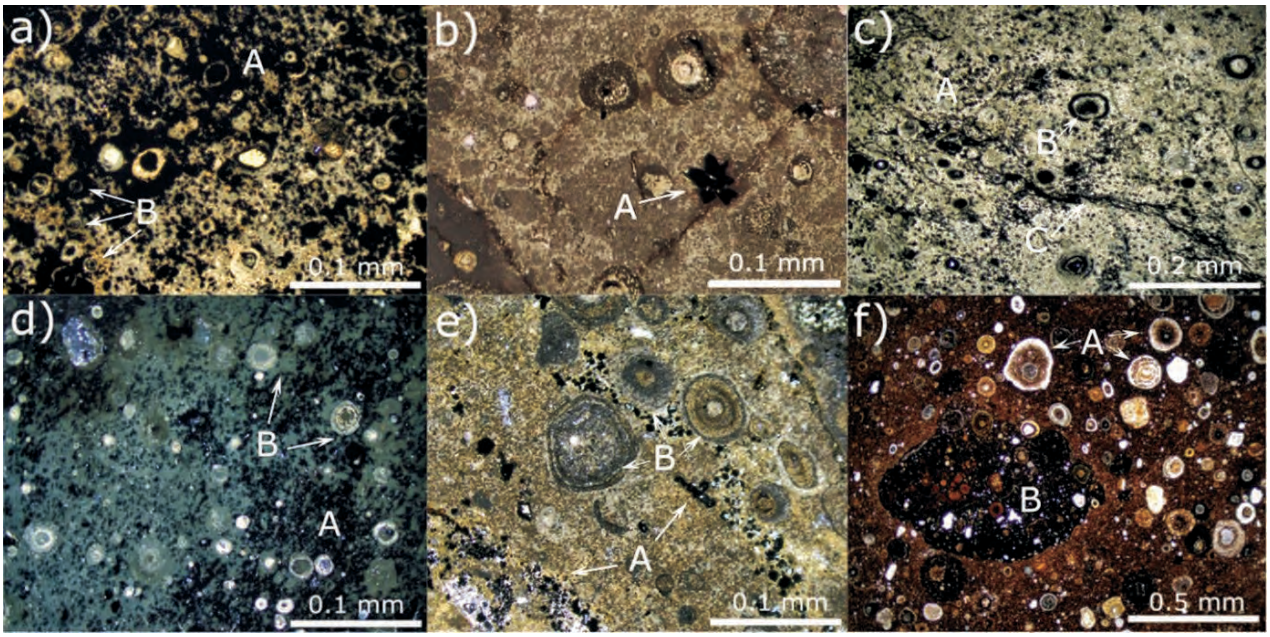

Fig. 18. Photomicrographs of different samples from the Minjera bauxites. (a) First generation of iron sulphides visible in the bauxite matrix (A) together with iron sulphides replacing the iron oxide rich lamellae in the ooids (B), D-1 deposit, PPL. (b) Completely deferrified section of the sample, with visible opaque marcasite rosette (A), D-15 deposit, PPL. (c) Clusters of iron sulphide framboids (A) in the bauxite matrix, iron sulphide rich lamellae in the ooids (B) and iron sulphide veins (C), D-1 deposit, PP. (d) Iron sulphides in the matrix of the bauxite (A), surrounding the diasporitic ooids (B), D-1 deposit, XPL. (e) Iron sulphide framboids (A) together with deferrified bauxite matrix and boehmitic ooids (B), D-15 deposit, PPL. (f) Ooids showing iron oxide rich and deferrified lamellae (A) together with iron oxide rich pebbles (B), red bauxite (MN-25), PPL.

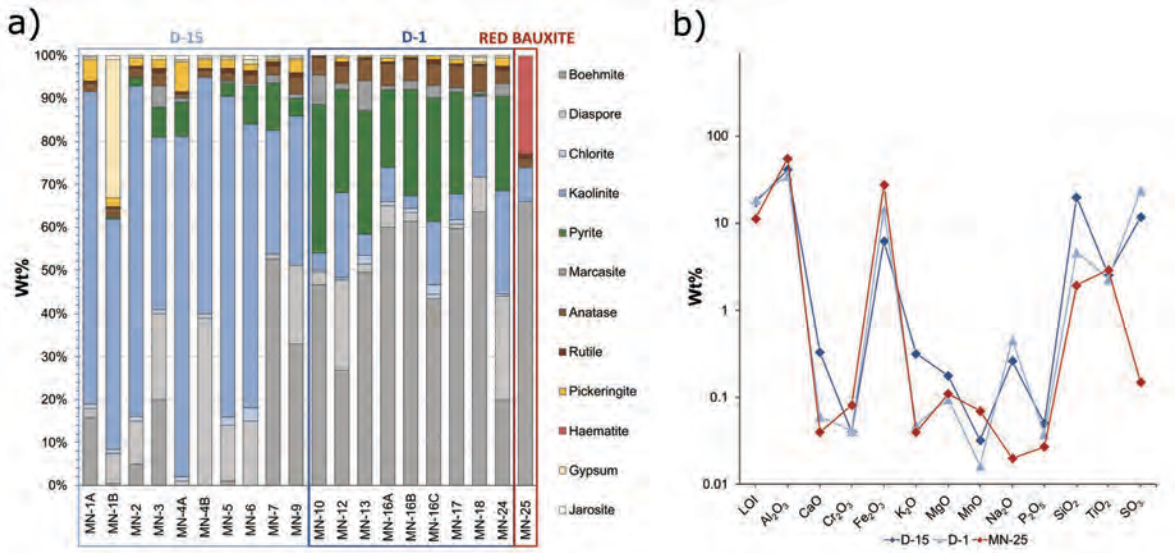

Fig. 19. Plots displaying the mineralogical composition and major oxide composition of the examined samples from the Minjera bauxite deposits D-15 and D-1 as well as the red bauxite sample. (a) Plot displaying the mineralogical composition of the examined samples. (b) Plot displaying the average major oxide composition of the samples from the deposits D-15 and D-1 as well as the values of the red bauxite sample.

deposit are located on the northern bank of the Mirna river, while the smaller canyon-type deposits and sinkhole-type deposits are found on the southern bank of the Mirna river, which probably indicates a higher palaeotopographical position of the bauxite bodies on the northern bank, allowing the formation of deeper karst structures with a stronger fluid flow and leading to more intense leaching during bauxitization.

The morphology of the iron sulphides is particularly diverse in the D-1 deposit and can be divided into several types. The first type of iron sulphides occurs as groups of crystal rosettes and anhedral aggregates that replace the bauxite matrix between the ooids and bauxite pebbles (Fig. 18a–e). The second type involves the replacement of iron oxide-rich lamellae in the ooids by iron sulphides (Fig. 18a, c). Iron sulphides replacing iron oxides in embedded bauxite pebbles represent the third type, while the last type includes iron sulphide veins cutting through previously formed structures (Fig. 18c), textures, and iron sulphide types. This is also visible on a large scale within the D-1 deposit, as centimetre-thick bands of iron sulphides parallel to the bedrock frequently occur in the bauxite of this deposit, indicating structural control dur-

ing its formation. All of these textures are visible in the D-15 deposit, although less common due to the lower iron sulphide content, and correspond to those described in the D-15 deposit by ŠINKOVEC et al. (1994). The required reducing environment and hydrogen sulphide were produced by reducing pore waters formed in the swamp that formed in the cover of the bauxite. Part of the sulphur probably came from decomposition of organic matter, while most of it was probably derived from microbial reduction of marine-derived sulphate as the marine influence is evident in certain sections of the overlying Kozina beds (ŠINKOVEC et al., 1994). When the bauxite was mostly consolidated after burial, overburden pressure caused fracturing of the bauxite, with iron sulphides crystallising along the newly formed fractures by reaction of undissolved iron oxides with the remaining pore water.

STOP 4 – TERRA ROSSA SOIL PROFILE IN THE KORONIKI VINEYARD: UPPER EOCENE–RECENT UNCONFORMITY

Terra rossa, the term introduced by TUĆAN (1912), is a generic term that refers to a soil formed in a Mediterranean climate that is red in colour, well-structured, high in Fe oxides strongly associated with clay minerals and overlying carbonate rocks (PRIORI et al., 2008). The term is commonly used by pedologists, geologists, archaeologists, geomorphologists, and sedimentologists in the Mediterranean region and in areas with continuously humid climates in the Western (e.g., Caribbean, Indiana, Wisconsin) and Eastern Hemispheres (e.g., southern Australia). In the WRB classification system, terra rossa soils can be classified as Cambisols, Luvisols, Nitisols (PRIORI et al., 2008), Leptosols (e.g., MUHS et al., 2010), and Lixisols (DURN et al., 2023). However, terra rossa is also referred to as a relict soil, polygenetic soil, palaeosol, pedosediment vetusol, lithified palaeosol, pedosedimentary complex, soil sediment, and sediment by various researchers (e.g., CREMASCHI, 1987; MIRABELLA et al., 1992; ALTAY, 1997; BENAC & DURN, 1997; BRONGER & BRUHN-LOBIN, 1997; DURN et al., 1999, 2007, 2014, 2018, 2023; DURN, 2003: FEDOROFF & COURTY, 2013; ZHANG et al., 2018; JONES, 2021; TRAVÉ et al., 2021).

The terra rossa soils on the Istrian peninsula, an archetypal example of a non-isolated karst area influenced by karst processes, (neo-)tectonic activity and input of external materials, are extensively studied polygenetic relict soils or palaeosols with a high content of crystalline iron oxides, composed mainly of haematite and sporadically of goethite, with kaolinite and illitic material representing the main clay mineral phases and nanosized mineral fraction dominated by authigenic kaolinite (DURN et al., 1999, 2001, 2007, 2013, 2014, 2019, 2021, 2023). They overlie and mark the youngest subaerial unconformity in the northwestern part of the Adriatic Carbonate Platform and are susceptible to erosional and redepositional processes. Terra rossa in Istria and generally in the northern Adriatic, fills cracks in karstified limestones (Fig. 20a) and forms a discontinuous surface layer up to several meters thick, which in favorable locations has been used for grape and olive cultivation since Roman times (Fig. 20b). It is also recognised as red polygenetic soil (Fig. 20c), red pedosedimentary complex (Fig. 20d, e), red palaeosol (Fig. 20f, g), and red lithified palaeosol (Fig. 20h). Terra rossa soils represent a valuable archive of information that can be used to understand present and past soil formation processes related to climate variability and landscape dynamics, especially in low-lying parts of the karst landscape where thicker deposits are typically found.

The provenance analysis revealed that the terra rossa allochthonous material originated mainly from the submerged alluvial plain/emerged Adriatic shelf, with two distinct signatures, i.e. Alpine/Apenninic area and Eocene flysch as dominant sources (RAZUM et al., 2023). Other less distinctive source materials include insoluble carbonate

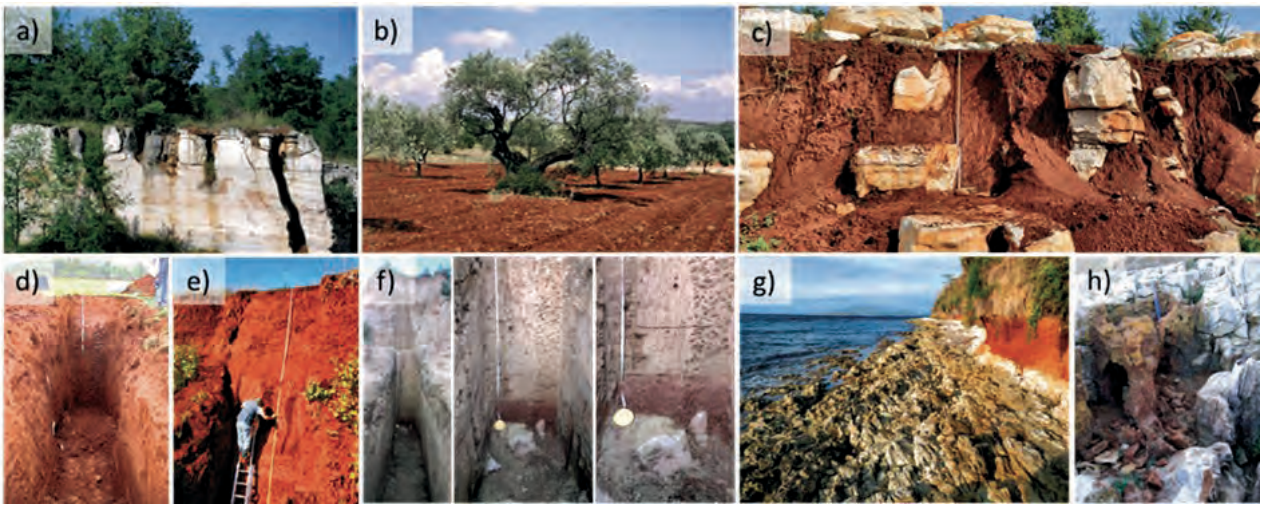

Fig. 20. The appearance of terra rosa soil in Istria and in the northern Adriatic. (a) Terra rossa filling of karstified cracks, Seline. (b) Terra rossa as a substrate for olive cultivation, Novigrad. (c) Red polygenetic soil, Kanfanar. (d) Red pedosedimentary complex, Koreniki. (e) Red pedosedimentary complex, Rovinj. (f) Red palaeosol at the base of an eight-meter-thick loess-palaeosol sequence, Savudrija. (g) Red palaeosol, Susak island and (h) Red lithified palaeosol, Susak island.

residue, tephra, and bauxite material. It is concluded that on a global scale terra rossa is most pronounced on the eastern Adriatic coast, because of the availability of siliciclastic material that was eroded in the Adriatic basin and regularly blown off the emerged shelf surface during periods of low sea levels (Fig. 21). The formation of terra rossa soils in the eastern Adriatic is a recurrent process that has started at least during the Miocene, while the aeolian transport from the emerged shelf may have begun even earlier, during the Oligocene (RAZUM et al., 2023).

Location

The studied soil profile is located on the southwestern Istrian planation surface, called "Red Istria" due to the widespread terra rossa soils, in a vineyard near the village of Koreniki (Fig. 22). On the highly generalized FAO-UNESCO Soil Map of Croatia (scale 1:1,000,000 – BOGUNOVIĆ et al., 1998), "Red Istria" includes almost exclusively Chromic Luvisols and Chromic Cambisols (in places associated with Mollic Leptosols, Dystric/Eutric Cambisols, Albic Lixisols and Anthrosols). The climate of the study region is often described simply as Mediterranean. However, since there are no significant differences in precipitation between seasons, it is actually humid subtropical climate (Cfa) according to the Köppen classification. The soil profile was studied on the site of a grass-covered vineyard in a soil pit excavated to a depth of three meters to the contact with the lower Eocene limestone (Fig. 22a, b). The surface of the limestone, at the point of contact with the soil, appears soft and moist. Occasional weathered limestone boulders and clasts are found in the soil at the contact with the limestone (Fig. 22b). The soil was described and sampled in accordance with FAO (2006) and IUSS Working Group WRB (2022). Details of sampling and analytical methods performed can be found in DURN et al. (2023).

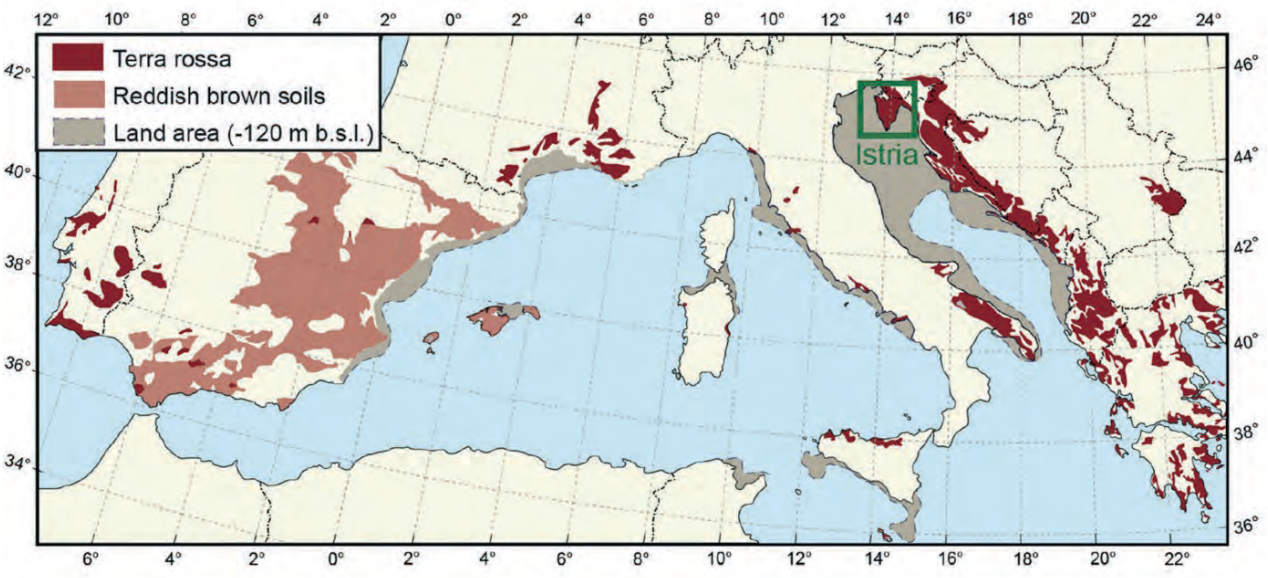

Fig. 21. Distribution map of terra rossa soils and surface shelf during the low sea levels. Large occurrences of terra rossa in the eastern Adriatic are associated with the large shelf area that, when emerged, provided siliciclastic material for terra rossa formation. Although this map shows the most recent palaeogeographic situation, large shallow shelf of the eastern Adriatic coast was probably formed in Oligocene (POPOV et al., 2004), thus from that age, recurrent aeolian transport of emerged shelf material onto the carbonate platform is probable (from RAZUM et al., 2023).

Fig. 22. (a) Terra rossa soil profile located in a vineyard at Koreniki (northwest coast of the Istrian peninsula, Croatia). (b) Cleaned terra rossa soil profile overlying a lower Eocene foraminifera limestone (marked by white arrow) with Ap, Ap/Bt1, Bt1, Bt2, 2Btb1, 2Btb2, 3Btb3 and 3Btb4 horizons.

Pedology and micromorphology

The studied profile has eight soil horizons (Fig. 22b) overlying lower Eocene limestone. All horizons are non-calcareous. The overall depth and general morphology of this profile suggest intense weathering and pedogenesis. The boundaries between soil horizons appear mostly smooth and gradual, except between the Ap and Ap/Bt horizons, where the Ap horizon abruptly and, at places, discontinuously overlies the Ap/Bt horizon. This is due to the soil disturbance by tillage (to a depth of 30–40 cm) and vine roots. In general, the soil becomes redder with increasing depth, indicating an increase in iron content. The soil texture is predominantly clay and generally becomes finer with increasing soil depth. Despite the high clay content, the soil morphology does not indicate significant water stagnation in this profile. The entire profile can be considered porous. Examination of the profile for redoximorphic soil features (mottling) revealed very few to few concentrations of Fe (and possibly Fe/Mn) (Fig. 22b). Due to intense weathering and pedogenesis, pH and CEC values are very low throughout the profile (Fig. 23a). Discontinuities in clay distribution at 170 cm and 230 cm depth (Fig. 23b) suggest that at least two major erosion and sedimentation cycles were involved in the formation of this soil profile, such that a more recent soil (0–170 cm) now overlies the remains of two older, i.e., more relict, soils (2Btb horizon from 170 to 230 cm and 3Btb horizon from 230 to 300 cm depth). A detailed description of the soil pedology and micromorphology can be found in DURN et al. (2023).

The groundmass is generally yellowish red or reddish in the topsoil and becomes distinctly red with increasing depth (in PPL). Microaggregation observed in the thin sections increases with soil depth. The redoximorphic features of the soil in the studied thin sections are usually few and very fine and consist of iron hypocoatings and infillings, depletion hypocoatings, more or less rounded, typic, orthic, and moderately Fe-impregnated nodules, and concentric, strongly impregnated, disorthic and anorthic Fe nodules with sharp boundaries (Fig. 24a). Their abundance does not follow a clear, gradual trend in the profile. In relation to the increasing clay content, the ratio of coarse to fine material of the groundmass (c/f ratio) is about 1:3 in the upper horizons (Fig. 24a) and decreases significantly in the lower horizons (Fig. 24e, f). The coarse fraction consists mainly of coarse silt-sized minerals (mainly quartz, followed by micas and rare quartzite grains). Bauxite clasts and quartz rosette grains were observed in a few samples, indicating colluvial transport from the surrounding area.

The clasts of red soil material (pedorelics) which are often incorporated within the generally less red groundmass suggests that colluvial and aeolian contribution of allochthonous soil material probably played a crucial role in the formation of this profile. The discontinuity between the more recent soil horizons (from Ap to Bt2) and the underlying older horizons (the pedosedimentary layers 2B and 3B), initially identified by the distribution of clay content, is clearly visible in the abrupt change of the groundmass at the Bt2/2Btb1 interface (Fig. 24b). Apart from the Ap horizon, more than 1% textural pedofeatures (mainly clay coatings and infillings) were detected in thin sections, confirming the argic nature of these soil horizons. In gen-

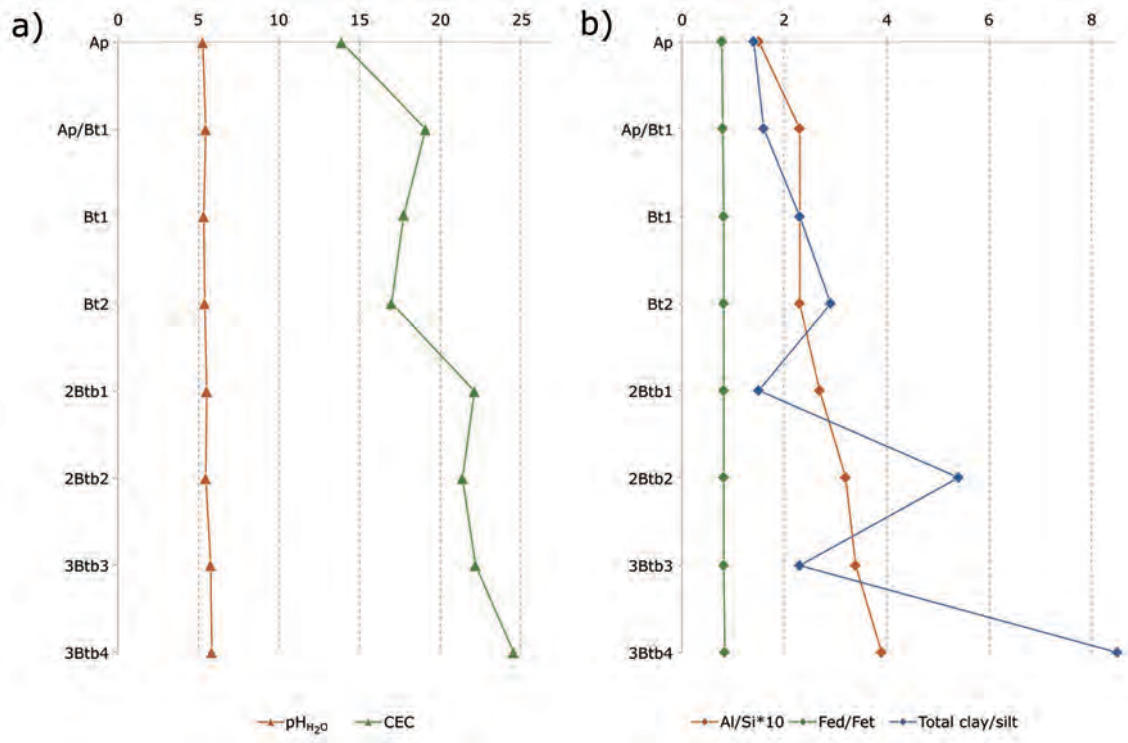

Fig. 23. (a) Distribution of pH_{H_2O} and CEC (cation exchange capacity of the bulk soil) at Koreniki profile. (b) Distribution of Al/Si(*10) ratio, Fe_d/Fe_t ratio (Fe_d – Na-dithionite-citrate-bicarbonate-extractable iron, Fe_t – total iron) and total clay/silt ratio at Koreniki profile.

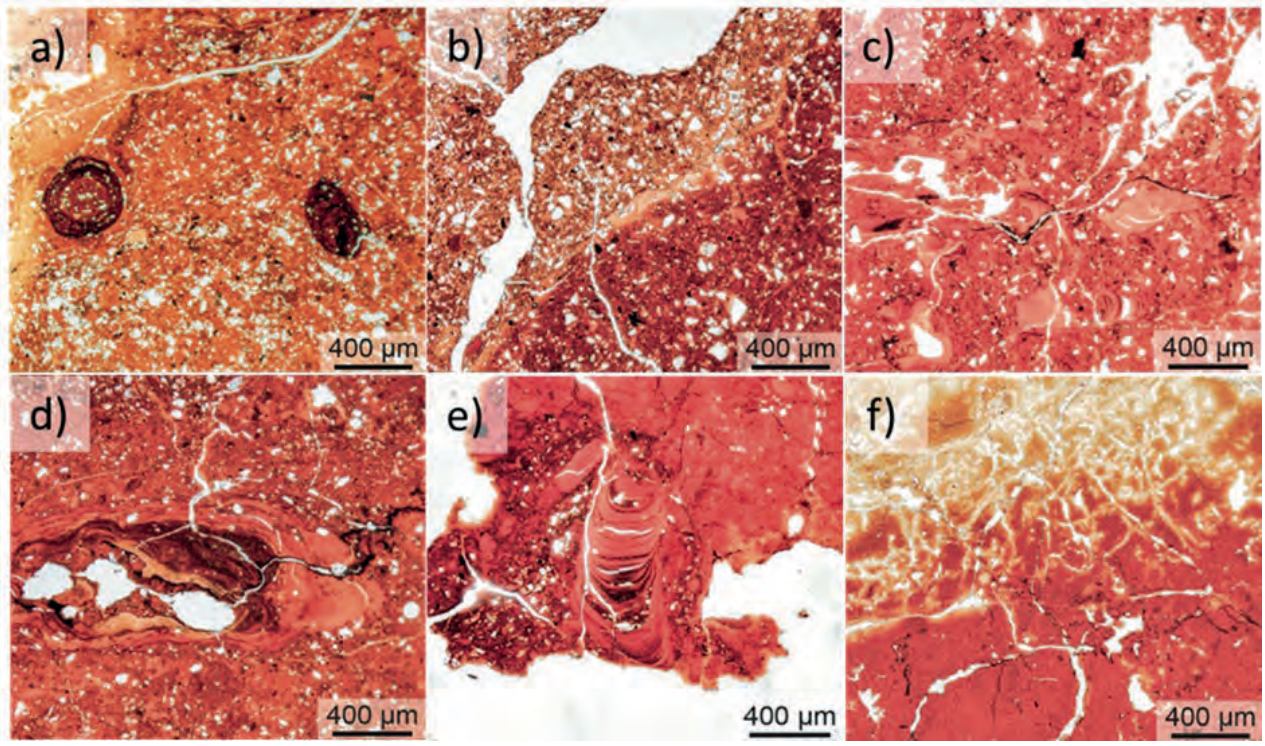

Fig. 24. Photomicrographs of the Koreniki soil profile. (a) Photomicrograph of the Bt2 horizon (PPL). The groundmass is dense and yellowish red. Dominant pedofeatures are nodules strongly impregnated by iron. (b) Photomicrograph (PPL) of the Bt2 horizon (boundary with the 2Btb1 horizon, PPL). Blocky microstructure with accommodated and partially accommodated subangular peds is well developed. Partially relict, dusty clay coatings/infillings are visible along the plane void that forms the abrupt boundary between the Bt2 and 2Btb1 horizons. (c) Photomicrograph of the 2Btb1 horizon (PPL). Microstructure is complex but dominated by planes along which clear clay coatings and infillings developed together with ferromanganese coatings and infillings. (d) Photomicrograph of the 2Btb2 horizon (PPL). The main feature is the alternation of limpid, dusty, and impure clay coatings, with depletion hypocoating overprinting the older illuviated material altogether truncated by younger illuviated material. (e) Photomicrograph of the 3Btb4 horizon (PPL). The groundmass in the upper right quadrant of the photo is denser (finer) than the remaining less dense, coarser groundmass; however, the coarser groundmass incorporates clasts of the material comprising the finer groundmass. In the center of the photo a large, crescent, complete infilling of limpid, dusty, and impure clay coatings is visible. (f) Photomicrograph of the 3Btb4 horizon (XPL). Complex microstructure mostly comprises accommodated angular peds separated by planes and occasionally channels forming a pore network coated with pure clay.

eral, the abundance of illuvial clay increases with the depth of the studied profile. The corresponding features include both pure illuvial clay coatings/infillings (Fig. 24c) and impure coatings of clay and silt (Figs. 24d, e). Both recent and relict illuvial pedofeatures were recognised, with the latter generally impure, deformed, and/or isolated within the former voids (Fig. 24e).

Geochemistry and mineralogy

The Al/Si ratio increases with depth from the Ap horizon to the 3Btb4 horizon and generally agrees with the increase in clay content (Fig. 23b), indicating that lessivage is a very important pedogenic process in the studied soil. Both Fe_t and Fe_d follow the distribution of Al/Si along the profile and show a continuous increase from the Ap horizon to the 3Btb4 horizon (DURN et al., 2023). The Fe_d/Fe_t ratio ranges from 0.79 in the Ap horizon to 0.85 in the 3Btb4 horizon, reflecting a very high degree of weathering of the Fe-bearing primary silicates (Fig. 23b). Due to the very high Fe_d/Fe_t ratio, the investigated soil is one of the most weathered terra rossa in Istria studied so far.

The main mineral phases in the < 2 mm fraction of all horizons are phyllosilicates, followed by quartz and haematite, while plagioclase, K-feldspar, and anatase are the minor mineral phases (Fig. 25a). The predominant mineral phase in the phyllosilicate group is kaolinite, followed by muscovite/illite, chlorite is a minor constituent, while paragonite occurs in trace amounts in the upper three horizons (Fig. 25a). While kaolinite and haematite show a continuous increase from the Ap horizon to the 3Btb4 horizon, quartz and chlorite show an opposite trend (Fig. 25a). Muscovite/illite, plagioclase, and anatase are uniformly distributed with depth (Fig. 25a). The distribution of kaolinite and haematite agrees with the distribution of Al/Si ratio, Fe_t and Fe_d, clearly indicating an increasing degree of weathering with depth and the process of lessivage.

The predominant mineral phase in the clay fraction is kaolinite, followed by illite, and hydroxy-interlayered mineral (HIM) is present in trace amounts (Fig. 25b, HIM is not shown). The kaolinite content shows a clear trend and increases from the Ap horizon to the 3Btb4 horizon (from 76 to 92 %). Illite content shows an opposite trend and decreases with depth (Fig. 25b). The presence of kaolinite and haematite in the studied profile and the absence of chlorite in the clay fraction may indicate that chlorite (together with feldspars, mica, and illite) was one of the main precursors for the formation of authigenic kaolinite and the

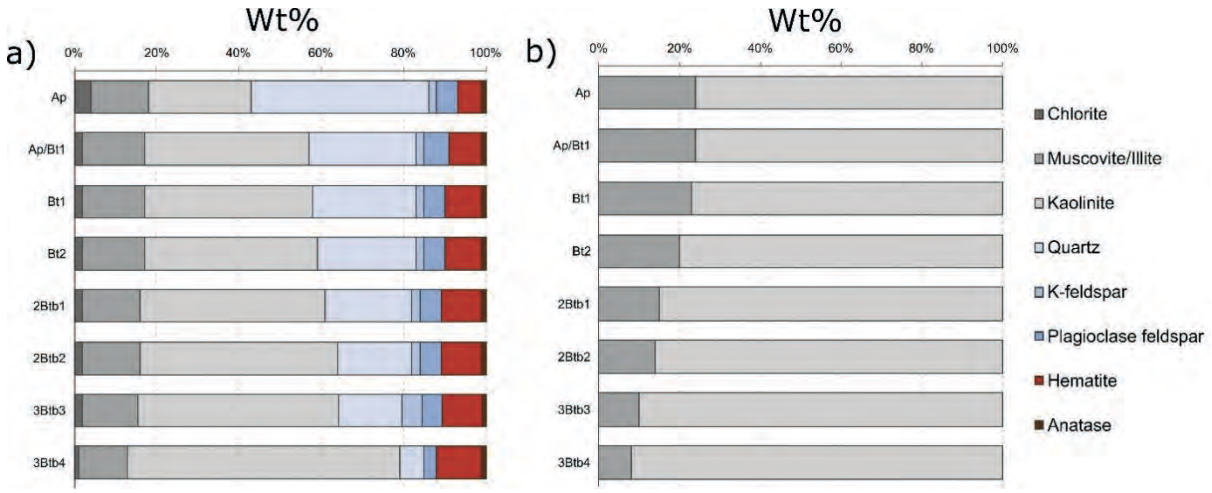

Fig. 25. (a) Mineral composition of the < 2 mm fraction at Koreniki profile (in mass %). (b) Mineral composition of the < 2 μm fraction at Koreniki profile (in mass %).

main source for the formation of iron oxides (haematite). The predominance of kaolinite in the clay fraction and clear evidence for the in situ growth of pedogenic kaolinite nanoparticles (DURN et al., 2023) suggest that kaolinisation, together with the formation of iron oxide (high Fe_d/Fe_t ratio), is a dominant process in the studied profile. Both processes complement ferralitisation, i.e., ferrallitic weathering. A detailed description of the soil geochemistry and mineralogy can be found in DURN et al. (2023).

Soil classification

According to the IUSS Working Group WRB (2022), the studied profile is classified as Rhodic Lixisol (Clayic, Aric, Cutanic). Lixisols are soils with pedogenetic clay differentiation (especially due to clay migration) between a topsoil with lower clay content and a subsoil with higher clay content, low activity clays (mainly kaolinite), and high base saturation at some depth (IUSS Working Group WRB, 2022). Lixisols are found in tropical, subtropical, and warm-temperate regions across Pleistocene and older surfaces – they occur mostly in the (sub)Sahelian and East Africa, but also in South and Central America, the Indian subcontinent, and Southeast Asia and Australia (IUSS Working Group WRB, 2022). Accordingly, the identification of a Lixisol in Istria represents a rare finding.

DURN et al. (2023) concluded that the finding of a Lixisol in the study area indicates the old age of the surface of the karst depression and provides the first data on the burial history of the southwestern Istrian planation surface. This suggests that some terra rossa soils previously classified as Cambisols or Luvisols may actually be Lixisols or other tropical soils (e.g., Nitisols) with preserved relict properties. DURN et al. (2023) also suggested that favourable periods for the formation of the studied soil in the northernmost part of the Mediterranean were older Quaternary interglacials, the mid-Piacenzian Warm Period (Pliocene), and/or the Miocene Climatic Optimum.

Acknowledgement

The work was supported by the Croatian Science Foundation under the project "Western Istrian Anticline as an Ideal Natural Laboratory for the Study of the Regional Unconformities in Carbonate Rocks – WianLab" (IP-2019-04-8054).

References

ALONSO-ZARZA, A.M., WRIGHT, V.P. (2010): Calcretes. In: Alonso-Zarza, A.M., Tanner, L.H. (eds.): Developments in Sedimentology. Elsevier, Oxford, pp. 225–267.

ALTAY, I. (1997): Red Mediterranean soils in some karstic regions of Taurus mountains, Turkey. Catena, 28, 247–260. https://doi.org/10.1016/S0341-8162(96)00041-0.

BARDOSSY, G. (1982): Karst bauxites, bauxite deposits on carbonate rocks. In: Development in Economic Geology, no. 14, vol. 1, Elsevier, Amsterdam.

BÁRDOSSY, G.Y., DERCOURT, J. (1990): Les gisements des bauxites Tethysiennes (Mediterranée, Proche et Moyen Orient): Cadre paléogeographique et controls genetiques. Bull. Soc. Geol. France, 8 (4/6), 869–888.

BENAC, Č., DURN, G. (1997): Terra rossa in the Kvarner area – geomorphological conditions of formation. Acta Geographica Croatica, 32, 7–19.

BERNOULLI, D. (2001): Mesozoic–Tertiary carbonate paltforms, slopes and basins of the external Appennines and Sicily. In: Vai, G.B., Martini, I.P. (eds): Anatomy of an Orogen: the Appennines and Adjacent Mediterranean Basins. Kluwer Academic Publ., 307–326.

BOGUNOVIĆ, M., VIDAČEK, Ž., RACZ, Z., HUSNJAK, S., ŠPOLJAR, A., SRAKA, M. (1998): FAO/UNESCO Croatian soil map, small scale 1:1.000,000, University of Zagreb, Faculty of Agriculture, project Monitoring Agriculture with Remote Sensing.

BRIGAUD, B., PUCÉAT, E., PELLENARD, P., VINCENT, B., JOACHIMSKI, M. M. (2008): Climatic fluctuations and seasonality during the Late Jurassic (Oxfordian–Early Kimmeridgian) inferred from $\delta^{18}O$ of Paris Basin oyster shells. Earth Planet. Sci. Lett., 273 (1–2), 58–67.

BRONGER, A., BRUHN-LOBIN, N. (1997): Paleopedology of terrae rossae – Rhodoxeralfs from Quaternary calcarenites

in NW Morocco. Catena, 28, 279–295. https://doi.org/10.1016/S0341-8162(96)00043-4.

CHANNELL, J.E.T. (1996): Paleomagnetism and paleogeography of Adria. Geol. Soc. London, Spec. publ., 105, 119–132.

CREMASCHI, M. (1987): Paleosols and Vetusols in the Central Po plain, a study in Quaternary Geology and Soil Development. Edizioni Unicopli, Milano, 306 p.

CVETKO TEŠOVIĆ, B., GLUMAC, B., BUCKOVIĆ, D. (2011): Integrated biostratigraphy and carbon isotope stratigraphy of the Lower Cretaceous (Barremian to Albian) Adriatic–Dinaridic carbonate platform deposits in Istria, Croatia. Cretaceous Research, 32, 3, 301–324.

D'AMBROSI, C. (1926): Rapporti tra morfologia e transgresioni nel Cretaceo e nel terziario dell'Istria. Atti Acc. Scient. Veneto-Trentina-Istriana, 16(3), 90–98.

D'ARGENIO, B., MINDSZENTY, A. (1995): Bauxites and related paleokarst: Tectonic and climatic event markers at regional unconformities. Eclogae Geologicae Helvetiae, 88, 453−499.

DECONINCK, J.F., STRASSER, A., DEBRABANT, P. (1988): Formation of illitic minerals at surface temperatures in Purbeckian sediments (Lower Berriasian, Swiss and French Jura). Clay minerals, 23, 91–103.

DOZET, S., MISIC, M., ZUZA, T. (1993): New data on the stratigraphic position, mineralogy and chemistry of Nanos bauxite deposits and adjacent carbonate rocks, Slovenia. Geol. Croat., 46(2), 233–241.

DRAGOVIĆ, D. (1989): The red and white karstic bauxites of Montenegro (Yugoslavia.). Trav. ICSOBA, 19(22), 249–257.

DURN, G. (2003): Terra rossa in the Mediterranean region: parent materials, composition and origin. Geol. Croat., 56 (1), 83–100.

DURN, G., OTTNER, F., SLOVENEC, D. (1999): Mineralogical and geochemical indicators of the polygenetic nature of terra rossa in Istria, Croatia. Geoderma, 91(1–2), 125–150.

DURN, G., SLOVENEC, D., ČOVIĆ, M. (2001): Distribution of iron and manganese in terra rossa from Istria and its genetic implications. Geol. Croat., 54 (1), 27–36. https://doi.org/10.4154/GC.2001.03.

DURN, G., OTTNER, F., TIŠLJAR, J., MINDSZENTY, A., BARUDŽIJA, U. (2003): Regional subaerial unconformities in shallow-marine carbonate sequences of Istria: sedimentology, mineralogy, geochemistry and micromorphology of associated bauxites, palaeosols and pedo-sedimentary complexes. In: Vlahović, I., Tišljar, J. (eds.): Evolution of Depositional Environments from the Paleozoic to the Quaternary in the Karst Dinarides and the Pannonian Basin. 22nd IAS Meeting of Sedimentology, Opatija, September 17-19, 2003, Field Trip Guidebook, 207–254.

DURN, G., OTTNER, F., MINDSZENTY, A., TIŠLJAR, J., MILEUSNIĆ, M. (2006): Clay mineralogy of bauxites and palaeosols in Istria formed during regional subaerial exposures of the Adriatic Carbonate Platform. In: Vlahović, I., Tibljaš, D., Durn, G. (eds.): 3rd Mid-European Clay Conference: Field Trip Guidebook, University of Zagreb, Faculty of Science and Faculty of Mining, Geology and Petroleum Engineering, 3–30.

DURN, G., ALJINOVIĆ, D., CRNJAKOVIĆ, M., LUGOVIĆ, B. (2007): Heavy and light mineral fractions indicate polygenesis of extensive terra rossa soils in Istria Croatia. In: Mange, M.A., Wright, D.T. (eds.): Heavy Minerals in Use. Developments in Sedimentology, vol. 58. Elsevier, pp. 701–737.

DURN, G., HRENOVIĆ, J., SEKOVANIĆ, L. (2013): Terra rossa as the substrate for biological phosphate removal from wastewater. Clay Miner., 48, 725–738. ttps://doi.org/10.1180/claymin.2013.048.5.05.

DURN, G., ČORIĆ, R., TADEJ, N., BARUDŽIJA, U., RUBINIĆ, V., HUSNJAK, S. (2014): Bulk and clay mineral composition indicate origin of terra rossa soils in Western Herzegovina. Geol. Croat., 67 (3), 171–183. https://doi.org/10.4154/GC.2014.13.

DURN, G., WACHA, L., BARTOLIN, M., ROLF, C., FRECHEN, M., TSUKAMOTO, S., TADEJ, N., HUSNJAK, S., LI, Y., RUBINIĆ, V. (2018): Provenance and formation of the red palaeosol and lithified terra rossa-like infillings on the Island of Susak: a high-resolution and chronological approach. Quat. Int., 494, 105–129. https://doi.org/10.1016/j.quaint.2017.11.040.

DURN, G., ŠKAPIN, S.D., VIDOVIĆ, N., RENNERT, T., OTTNER, F., RUŽIČIĆ, S., CUKROV, N., SONDI, I. (2019): Impact of iron oxides and soil organic matter on the surface physicochemical properties and aggregation of Terra Rossa and Calcocambisol subsoil horizons from Istria (Croatia). Catena, 183, 104184. https://doi.org/10.1016/j.catena.2019.104184.

DURN, G., PERKOVIĆ, I., STUMMEYER, J., OTTNER, F., MILEUSNIĆ, M. (2021): Differences in the behaviour of trace and rare-earth elements in oxidizing and reducing soil environments: Case study of terra rossa soils and Cretaceous palaeosols from the Istrian peninsula, Croatia. Chemosphere, 283, 131286. https://doi.org/10.1016/j.chemosphere.2021.131286.

DURN, G., PERKOVIĆ, I., RAZUM, I., OTTNER, F., ŠKAPIN, S.D., FAIVRE, S., BELOŠA, L., VLAHOVIĆ, I., RUBINIĆ, V. (2023): A tropical soil (Lixisol) identified in the northernmost part of the Mediterranean (Istria, Croatia). Catena, 228, 107–144. https://doi.org/10.1016/j.catena.2023.107144

ECONOMOU-ELIOPOULOS, M., KONTOU, M., MEGREMI, I. (2022): Biogeochemical Redox Processes Controlling the Element Cycling: Insights from Karst-Type Bauxite, Greece. Minerals, 12(4), 446.

FAO (2006): Guidelines for Soil Description, fourth ed. Food and Agriculture Organization of the United Nations, Rome.

FEDOROFF, N., COURTY, M.A. (2013): Revisiting the genesis of red Mediterranean soils. Tur. J. Earth Sci., 22, 359–375. https://doi.org/10.3906/yer-1205-10.

FRAKES, L.A., FRANCIS, J.E., SYKTUS, J.I. (1992): Climate Modes of the Phanerozoic, Cambridge University Press, Cambridge, 286.

GAMALETSOS, P.N., GODELITSAS, A., KASAMA, T., CHURCH, N.S., DOUVALIS, A.P., GÖTTLICHER, J., STEININGER, R., BOUBNOV, A., PONTIKES, Y., TZAMOS, E., BAKAS, T., FILIPPIDIS, A. (2017): Nano-mineralogy and -geochemistry of high-grade diasporic karst-type bauxite from Parnassos-Ghiona mines, Greece. Ore Geo. Rev., 84, 228–244.

GUŠIĆ, I., JELASKA V. (1993): Upper Cenomanian–Lower Turonian sea-level rise and its consequences on the Adriatic-Dinaric carbonate platform. Geologische Rundschau, 82, 678–686.

HANDY, M.R., SCHMID, S.M., BOUSQUET, R., KISSLING, E., BERNOULLI, D. (2010): Recoiling plate-tectonic reconstructions of Alpine Tethys with the geological-geophysical record of spreading and subduction in the Alps. Earth-Science Reviews 102(3), 121–158.

HAQ, B.U. (2018): Jurassic sea-level variations: A reappraisal. GSA Today, 28(1), 4–10.

HAQ, B.U., AL-QAHTANI, A.M. (2005): Phanerozoic cycles of sea-level change on the Arabian platform. GeoArabia, 10(2), 127–160.

HESSELBO, S.P., JEAN-FRANÇOIS, D., HUGGETT, J.M., MORGANS-BELL, H.S. (2009): Late Jurassic palaeoclimatic change from clay mineralogy and gamma-ray spectrome-

try of the Kimmeridge Clay, Dorset, UK. J. Geol. Soc, 166(6), 1123–1133.

HUCK, S., RAMEIL, N., KORBAR, T., HEIMHOFER, U., WIECZOREK, T.D., IMMENHAUSER, A. (2010): Latitudinally different responses of Tethyan shoal-water carbonate systems to the Early Aptian oceanic anoxic event. Sedimentology, 57 (7), 1585–1614.

IUSS WORKING GROUP WRB (2022): World Reference Base for Soil Resources. International soil classification system for naming soils and creating legends for soil maps. 4th edition. International Union of Soil Sciences (IUSS), Vienna.

JENKYNS, H.C. (1980): Cretaceous anoxic events: from continents to oceans. Journal of the Geological Society, 137, 171–188.

JENKYNS, H.C. (1991): Impact of Cretaceous sea-level rise and anoxic events in the Mesozoic carbonate platform of Yugoslavia. American Association of Petroleum Geologists, Bulletin, 75, 1007–1017.

JONES, B. (2021): Formation, dispersion and accumulation of terra rossa on the Cayman Islands. Sedimentology, 68, 1964–2008. https://doi.org/10.1111/sed.12841.

JONES, C.E., JENKYNS, H.C. (2001): Seawater strontium isotopes, oceanic anoxic events, and seafloor hydrothermal activity in the Jurassic and Cretaceous. American Journal of Science, 301, 112–149

LASKOU, M., ECONOMOU-ELIOPOULOS, M. (2007): The role of microorganisms on the mineralogical and geochemical characteristics of the Parnassos-Ghiona bauxite deposits, Greece. J. Geochem. Explor., 93(2), 67–77.

LASKOU, M., ECONOMOU-ELIOPOULOS, M. (2013): Bio-mineralization and potential biogeochemical processes in bauxite deposits: Genetic and ore quality significance. Mineral. Petrol., 107(4), 471–486.

MATIČEC, D., VLAHOVIĆ, I., VELIĆ, I., TIŠLJAR, J. (1996): Eocene limestones overlying Lower Cretaceous deposits of western Istria (Croatia): did some parts of present Istria form land during the Cretaceous? Geologia Croatica, 49 (1), 117–127.

MENAGATTI, A.P., WEISSERT, H., BROWN, R.S., TYSON, R.V., FARRIMOND, P.A.S., CARON, M. (1998): High-resolution $\delta^{13}C$ stratigraphy through the early Aptian "Livello Selli" of the Alpine Tethys. Paleoceanography, 13, 530–545.

MILEUSNIĆ, M. (2007): Podrijetlo, uvjeti nastanka i sastav glinovitih naslaga taloženih tijekom aptsko-albske emerzije u Istri. Unpubl. PhD Thesis, University of Zagreb, Faculty of Mining, Geology and Petroleum Engineering.

MINDSZENTY, A. (2004): On the controversial nature of paleosols related to shallow marine carbonate depositional environments. Slovenian Geological Society (SGD), Sedimentary Geological Section (SSG), "SSG seminar", ZRC SAZU, March 2004, Ljubljana.

MINDSZENTY, A. (2016): Bauxites: Feedbacks of System Earth at Greenhouse times. Geologia Croatica, 69(1), 79−87.

MIRABELLA, A., COSTANTINI, E.A.C., CARNICELLI, S. (1992): Genesis of a policyclic Terra Rossa (Chromic Cambisol on Rhodic Nitisol) at the Poggio del Comune in Central Italy. Z. Planzenernähr. Bodenkd., 155, 407–413. https://doi.org/10.1002/jpln.19921550510.

MOLINA, J.M., RUIZ-ORTIZ, P.A., ERA, J.A. (1991): Jurassic karst bauxites in the Subbetic, Betic Cordillera, southern Spain. Acta Geol. Hung., 34(3), 163–178.

MUHS, D.R., BUDAHN, J., AVILA, A., SKIPP, G., FREEMAN, J., PATTERSON, D.A. (2010): The role of African dust in the formation of Quaternary soils on Mallorca, Spain and implications for the genesis of Red Mediterranean soils. Quat. Sci. Rev., 29 (19–20), 2518–2543. https://doi.org/10.1016/j.quascirev.2010.04.013.

OTTNER, F. (1999): Herkunft und Zusammensetzung von Peliten der Unterkreide Istriens, Kroatien: Sedimente oder Paleoböden. Habilitationsschrift zur Erlangung der Venia legendi für das wissenschaftliche Fach Geologie, Vienna, 137.

PELLENARD, P., NOMADE, S., MARTIRE, L., DE OLIVEIRA RAMALHO, F., MONNA, F., GUILLOU, H. (2013): The first ^{40}Ar–^{39}Ar date from Oxfordian ammonite-calibrated volcanic layers (bentonites) as a tie-point for the Late Jurassic. Geol. Mag., 150(6), 1–7.

PRIORI, S., COSTANTINI, E., CAPEZZUOLI, E., PROTANO, G., HILGERS, A., SAUER, D., SANDRELLI, F. (2008): Pedostratigraphy of Terra Rossa and Quaternary geological evolution of a lacustrine limestone plateau in central Italy. J. Plant Nutr. Soil Sci., 171, 509–523. https://doi.org/10.1002/jpln.200700012 509.

RADUSINOVIĆ, S., PAPADOPOULOS, A. (2021): The potential for REE and associated critical metals in karstic bauxites and bauxite residue of Montenegro. Minerals, 11(9), 975.

RADUSINOVIĆ, S., JELENKOVIĆ, R., PAČEVSKI, A., SIMIĆ, V., BOŽOVIĆ, D., HOLCLAJTNER-ANTUNOVIĆ, I., ŽIVOTIĆ, D. (2017): Content and mode of occurrences of rare earth elements in the Zagrad karstic bauxite deposit (Nikšić area, Montenegro). Ore Geol. Rev., 80, 406–428.

RASMUSSEN, K., NEUMANN, A.C.N. (1988): Holocene overprint of Pleistocene paleokarst: Bight of Abaco, Bahamas. In: James, N.P., Choquette, P.W. (eds.): Paleokarst, Springer-Verlag, New York, 132–148.

RAZUM, I., RUBINIĆ, V., MIKO, S., RUŽIČIĆ, S., DURN, G. (2023): Coherent provenance analysis of terra rossa from the northern Adriatic based on heavy mineral assemblages reveals the emerged Adriatic shelf as the main recurring source of siliciclastic material for their formation. Catena, 107083. https://doi.org/10.1016/j.catena.2023.107083.

RETALLACK, G.J. (2010): Lateritization and bauxitization events. Economic Geology, 105, 655−667.

RUFFELL, A.H., RAWSON, P.F. (1994): Palaeoclimate control on sequence stratigraphic patterns in the late Jurassic to mid-Cretaceous, with a case study from Eastern England. Palaeogeogr., Palaeoclimatol., Palaeoecol., 110(1–2), 43–54.

SCHMID, S.M., BERNOULLI, D., FÜGENSCHUH, B., MATENCO, L., SCHEFER, S., SCHUSTER, R., TISCHLER, M., USTASZEWSKI, K. (2008): The Alpine-Carpathian-Dinaridic orogenic system: Correlation and evolution of tectonic units. Swiss J. Geosci., 101(1), 139–183.

SCHMID, S.M., FÜGENSCHUH, B., KOUNOV, A., MAŢENCO, L., NIEVERGELT, P., OBERHÄNSLI, R., PLEUGER, J., SCHEFER, S., SCHUSTER, R., TOMLJENOVIĆ, B., USTASZEWSKI, K., VAN HINSBERGEN, D.J.J. (2020): Tectonic units of the Alpine collision zone between Eastern Alps and western Turkey. Gondwana Res., 78, 308–374.

STAMPFLI, G.M., MOSAR, J. (1999): The making and becoming of Apulia. In: Gosso, G., Jadoul, F., Sella, M., Spalla, M.I. (eds.): 3rd Workshop on Alpine Geological Studies. Padova, Memorie di scienze Geologiche, 51/1, 141–154.

STEINER, T.M.C., GAWLICK, H.J., MELCHER, F., SCHLAGINTWEIT, F. (2021): Ophiolite derived material as parent rocks for Late Jurassic bauxite: evidence for Tithonian unroofing in the Northern Calcareous Alps (Eastern Alps, Austria). Int. J. Earth Sci., 110(5), 1847–1862.

ŠĆAVNIČAR, B., NIKLER, L. (1976): Vitric tuff in Upper Jurassic Lemeš-deposits of Mt. Velika Kapela (Croatia). Geol. Vj., 29, 269–275.

ŠINKOVEC, B. (1974): Jurski glinoviti boksiti zapadne Istre. Geol.Vj., 27, 217–226.

ŠINKOVEC, B., SAKAČ, K., DURN, G. (1994): Pyritized bauxites from Minjera, Istria, Croatia. Natura Croatica, 3, 41–65.

TIŠLJAR, J. (1978): Onkolitni i stromatolitni vapnenci u donjokrednim sedimentima Istre (Hrvatska, Jugoslavija). Geološki Vjesnik, 30, 363–382 (*with English abstract*).

TIŠLJAR, J. (1986): Postanak crnih oblutaka i ulomaka ("black pebbles") u periplimskim vapnencima titona zapadne Istre i barema otoka Mljeta. Geol. Vj., 39(75–94), 75–94.

TIŠLJAR, J., VLAHOVIĆ, I., MATIČEC, D., VELIĆ, I. (1995): Platformni facijesi od gornjeg titona do gornjeg alba u zapadnoj Istri i prijelaz u tempestitne, klinoformne i rudistne biolititne facijese donjega cenomana u južnoj Istri (ekskurzija B) (Platform Facies from the Upper Tithonian to Upper Albian in Western Istria and Transition into Tempestite, Clinoform and Rudist Biolithite Facies of the Lower Cenomanian in Southern Istria). In: Vlahović, I., Velić, I. (eds.): Excursion Guide-Book, First Croatian Geological Congress, Zagreb, Croatia, 67–110 (*with English summary*).

TRAVÉ, A., RODRÍGUEZ–MORILLAS, N., BAQUÉS, V., PLAYÀ, E., CASAS, L., CANTARERO, I., MARTÍN–MARTÍN, J.D., GÓMEZ–RIVAS, E., MORAGAS, M., CRUSET, D. (2021): Origin of the coloured karst fills in the Neogene extensional system of NE Iberia (Spain). Minerals, 11, 1382. doi: 10.3390/min11121382.

TROJANOVIĆ, D. (1973): Jurski boksiti zapadne Istre. II. Jugoslavenski Simpozij o Istraživanju i Eksploataciji Boksita, 53–66.

TUĆAN, F. (1912): Terra Rossa, deren Natur and Entstehung. Jahrbuch Min. Geol. Pal., XXXIV. Beilage, pp. 401–430.

VAN HINSBERGEN, D.J.J., TORSVIK, T.H., SCHMID, S.M., MAŢENCO, L.C., MAFFIONE, M., VISSERS, R.L.M., GÜRER, D., SPAKMAN, W. (2020): Orogenic architecture of the Mediterranean region and kinematic reconstruction of its tectonic evolution since the Triassic. Gondwana Res., 81, 79–229.

VELIĆ, I., TIŠLJAR, J. (1988): Litostratigrafske jedinice u dogeru i malmu zapadne Istre (zapadna Hrvatska, Jugoslavija). Geol. Vj., 41, 25–49.

VELIĆ, I., MATIČEC, D., VLAHOVIĆ, I., TIŠLJAR, J. (1995): Stratigrafski slijed jurskih i donjokrednih karbonata (bat–gornji alb) u zapadnoj Istri (ekskurzija A). (Stratigraphic succession of Jurassic and Lower Cretaceous (Bathonian–Upper Albian) in western Istria (Excursion A)). In: Vlahović, I., Velić, I. (eds.), Excursion Guide-Book, First Croatian Geological Congress, Zagreb, Croatia, 31–66 (*with English summary*).

VELIĆ, I., TIŠLJAR, J., SOKAČ, B. (1989): The variability of thicknesses of the Barremian, Aptian and Albian carbonates as a consequence of changing depositional environments and emersion in western Istria (Croatia, Yugoslavia). Memorie della Società Geologica Italiana, 40, 209–218.

VELIĆ, I., TIŠLJAR, J., VLAHOVIĆ, I., VELIĆ, J., KOCH, G., MATIČEC, D. (2002): Palaeogeographic Variability and Depositional Environments of the Upper Jurassic Carbonate Rocks of Velika Kapela Mt. (Gorski Kotar Area, Adriatic Carbonate Platform, Croatia). Geol. Croat., 55(2), 121–138.

VELIĆ, I., TIŠLJAR, J., VLAHOVIĆ, I., MATIČEC, D., BERGANT, S. (2003): Evolution of the Istrian Part of the Adriatic Carbonate Platform from the Middle Jurassic to the Santonian and Formation of the Flysch Basin during the Eocene: Main Events and Regional Comparison. In: Vlahović, I., Tišljar, J. (eds.): Evolution of Depositional Environments from the Palaeozoic to the Quaternary in the Karst Dinarides and the Pannonian Basin, Field Trip Guidebook, 22nd IAS Meeting of Sedimentology, Opatija, 3–17.

VLAHOVIĆ, I., TIŠLJAR, J., VELIĆ, I. (1994): Influence of synsedimentary tectonics and eustatic changes on deposition of the Cenomanian platform carbonates in Istria (Western Croatia). Géol. Médit., 21(3), 189–193.

VLAHOVIĆ, I., TIŠLJAR, J., VELIĆ, I., MATIČEC, D., SKELTON, P., KORBAR, T., FUČEK, L. (2003): Main Events Recorded in the Sedimentary Succession of the Adriatic Carbonate Platform from Oxfordian to the Upper Santonian in Istria (Croatia). In: Vlahović, I., Tišljar, J. (eds.): Evolution of Depositional Environments from the Palaeozoic to the Quaternary in the Karst Dinarides and the Pannonian Basin. 22nd IAS Meeting of Sedimentology, Opatija, September 17-19, 2003, Field Trip Guidebook, 19–58.

VLAHOVIĆ, I., TIŠLJAR, J., VELIĆ, I., MATIČEC, D. (2005): Evolution of the Adriatic Carbonate Platform: Palaeogeography, main events and depositional dynamics. Palaeogeogr., Palaeoclimatol., Palaeoecol., 220(3–4), 333–360.

WIGNALL, P.B., RUFFELL, A.H. (1990): The influence of a sudden climatic change on marine deposition in the Kimmeridgian of northwest Europe. J. Geol. Soc. (London, U.K.), 147(2), 365–371.

ZHANG, J., ROLF, C., WACHA, L., TSUKAMOTO, S., DURN, G., FRECHEN, M. (2018): Luminescence dating and palaeomagnetic age constraint of a last glacial loess–palaeosol sequence from Istria, Croatia. Quat. Int., 494, 19–33.